Article

Black hole jets on the scale of the cosmic web

https://doi.org/10.1038/s41586-024-07879-y

Received: 16 February 2024

Accepted: 25 July 2024

Published online: 18 September 2024

Check for updates

Martijn S. S. L. Oei[1,2]✉, Martin J. Hardcastle[3], Roland Timmerman[1,4], Aivin R. D. J. G. I. B. Gast[5], Andrea Botteon[6], Antonio C. Rodriguez[2], Daniel Stern[7], Gabriela Calistro Rivera[8,9], Reinout J. van Weeren[1], Huub J. A. Röttgering[1], Huib T. Intema[1], Francesco de Gasperin[6] & S. G. Djorgovski[2]

When sustained for megayears (refs. 1,2), high-power jets from supermassive black holes (SMBHs) become the largest galaxy-made structures in the Universe[3]. By pumping electrons, atomic nuclei and magnetic fields into the intergalactic medium (IGM), these energetic flows affect the distribution of matter and magnetism in the cosmic web[4–6] and could have a sweeping cosmological influence if they reached far at early epochs. For the past 50 years, the known size range of black hole jet pairs ended at 4.6–5.0 Mpc (refs. 7–9), or 20–30% of a cosmic void radius in the Local Universe[10]. An observational lack of longer jets, as well as theoretical results[11], thus suggested a growth limit at about 5 Mpc (ref. 12). Here we report observations of a radio structure spanning about 7 Mpc, or roughly 66% of a coeval cosmic void radius, apparently generated by a black hole between $4.4^{+0.2}_{-0.7}$ and 6.3 Gyr after the Big Bang. The structure consists of a northern lobe, a northern jet, a core, a southern jet with an inner hotspot and a southern outer hotspot with a backflow. This system demonstrates that jets can avoid destruction by magnetohydrodynamical instabilities over cosmological distances, even at epochs when the Universe was 7 to 15^{+6}_{-2} times denser than it is today. How jets can retain such long-lived coherence is unknown at present.

To quantify the impact of black hole energy transport on the IGM, radio images from the International LOFAR Telescope (ILT) have recently been searched (for example, refs. 9,13–15) for Mpc-scale galactic outflows. In particular, our team systematically scanned the continuing northern sky survey of the ILT at wavelength $\lambda = 2.08$ m both with machine learning and by eye—the latter with substantial contributions from citizen scientists[16]. This endeavour has increased the number of known Mpc-scale outflows from a few hundred to more than 11,000 (ref. 15). Our largest find is the outflow shown in Fig. 1 and Extended Data Fig. 1, which we name Porphyrion. The source, of angular length $\phi = 13.4' \pm 0.1'$, seems unusually thin. To investigate from which galaxy along the jet axis the outflow originates, we processed ILT very-long-baseline interferometry (VLBI) data of the central $4' \times 4'$. At a spatial resolution of 3 kpc, the image (Fig. 1a inset and Extended Data Fig. 2) shows lone, unresolved radio sources in two galaxies, in both cases implying active accretion onto an SMBH. Because the detection of jets near either black hole (and along the overarching NNE–SSW axis) would clarify the origin of Porphyrion, we performed deep follow-up observations with the upgraded Giant Metrewave Radio Telescope (uGMRT) at $\lambda = 0.46$ m. The resulting image and ancillary DESI Legacy Imaging Surveys (Legacy) optical–infrared data (Fig. 1b inset) reveal that the outflow protrudes from a massive ($M_\star = 6.7^{+1.4}_{-1.4} \times 10^{11}\ M_\odot$) galaxy. This is visually clear in Fig. 2, which is processed to highlight the radio morphologies of the two central galaxies. Of these, the southernmost galaxy uniquely shows a 5σ extension along the overarching jet axis of Porphyrion. We observed this galaxy with the Low Resolution Imaging Spectrometer (LRIS) on the W. M. Keck Observatory's Keck I telescope, measuring a spectroscopic redshift $z = 0.896 \pm 0.001$ (Fig. 3a). We witness Porphyrion at $t_{BB} = 6.3$ Gyr after the Big Bang.

The angular length and redshift of the outflow entail a sky-projected length $l_p = 6.43 \pm 0.05$ Mpc. This makes Porphyrion the projectively longest known structure generated by an astrophysical body. The total length of the outflow exceeds this projected length, but by how much depends on the unknown inclination of the jets with respect to the sky plane. Deprojection formulae[14] predict a total length $l = 6.8^{+1.2}_{-0.3}$ Mpc, with expectation $\mathbb{E}[L|L_p = l_p] = 7.28 \pm 0.05$ Mpc (Methods). We thus estimate Porphyrion to be about 7 Mpc long in total. Spanning about 66% of the radius of a typical cosmic void at its redshift, the outflow is truly cosmological. Surprisingly, SMBH jets can remain collimated over several megaparsecs, despite the growth of (magneto) hydrodynamical instabilities—mainly Kelvin–Helmholtz instabilities—predicted theoretically and seen in simulations of shorter jets (for example, ref. 11). Similarly, prolonged entrainment of mass from the IGM, even at $z \gtrsim 1$, does not necessarily destabilize jets. No magneto-hydrodynamical simulations of Mpc-scale jets yet exist: the spatio-temporal grids required imply a numerical cost roughly 10^2 times higher than that of state-of-the-art runs. Outflows such as Porphyrion thus offer a window into a jet physics regime that, at present, cannot be explored numerically.

Active galactic nuclei (AGN) with accretion disks extending to the innermost stable circular orbits of their SMBHs efficiently convert the gravitational potential energy of infalling matter into radiation and are thus called radiatively efficient (RE); all others are called radiatively inefficient (RI)[17,18]. In RE AGN, the luminous accretion disk photo-ionizes

[1]Leiden Observatory, Leiden University, Leiden, The Netherlands. [2]Cahill Center for Astronomy and Astrophysics, California Institute of Technology, Pasadena, CA, USA. [3]Centre for Astrophysics Research (CAR), University of Hertfordshire, Hatfield, United Kingdom. [4]Centre for Extragalactic Astronomy, Department of Physics, Durham University, Durham, United Kingdom. [5]Somerville College, University of Oxford, Oxford, United Kingdom. [6]INAF–IRA, Bologna, Italy. [7]Jet Propulsion Laboratory, California Institute of Technology, Pasadena, CA, USA. [8]European Southern Observatory, Garching bei München, Germany. [9]Institute of Communications and Navigation, German Aerospace Center (DLR), Weßling, Germany. ✉e-mail: oei@caltech.edu

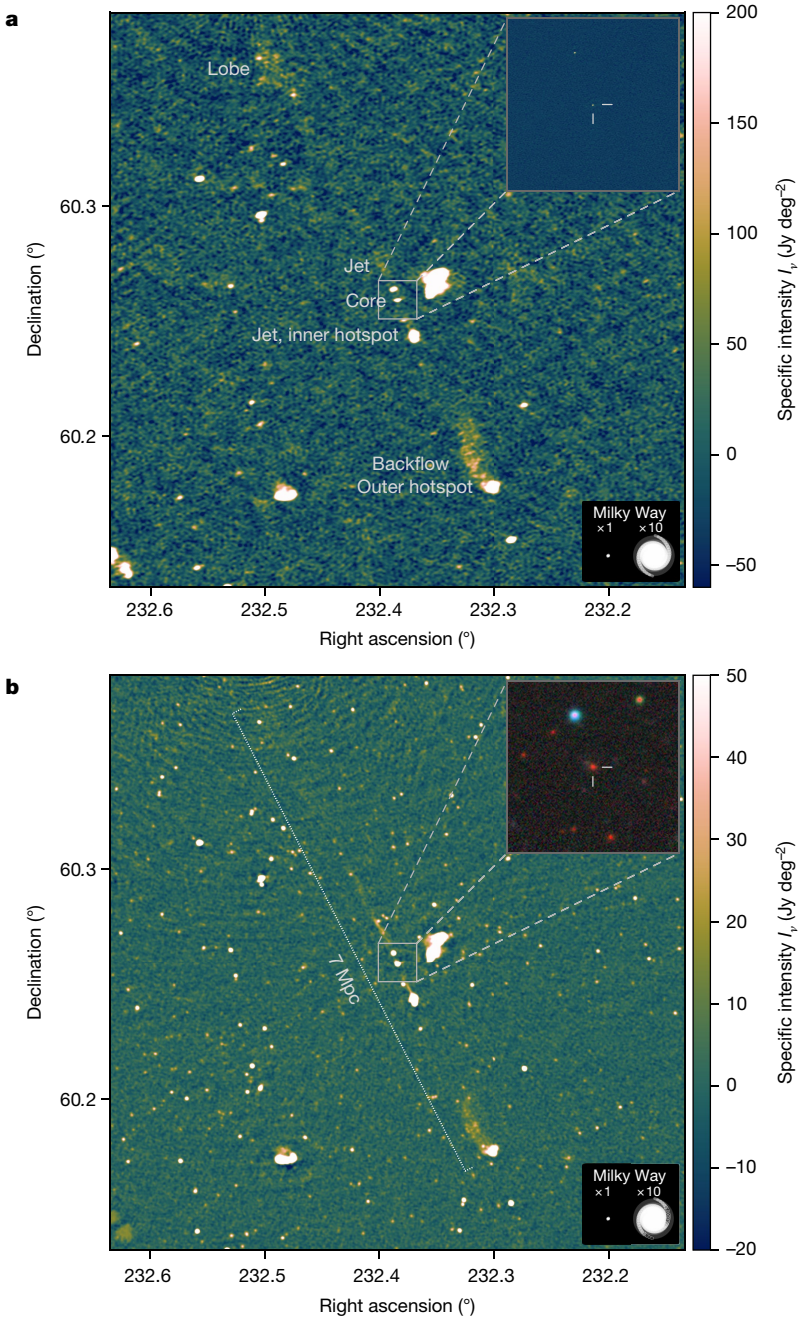

Fig. 1 | Deep radio images of a 7-Mpc-long, black-hole-driven outflow. **a**,**b**, These images were taken with the ILT and uGMRT at central wavelengths $\lambda = 2.08$ m and $\lambda = 0.46$ m, respectively, and have resolutions of 6.2″ and 4.3″, respectively. Panel **a** inset shows ILT VLBI imagery at $\lambda = 2.08$ m and a resolution of 0.4″. Panel **b** inset shows Legacy Surveys DR10 optical–infrared imagery. The larger images cover 15′ × 15′ of sky, whereas the insets cover 1′ × 1′. For scale, we show the stellar Milky Way disk (diameter: 50 kpc) and a ten times inflated version.

a circumnuclear region emitting narrow, and often forbidden, spectral lines. The Keck-observed prominence of forbidden ultraviolet–optical lines from oxygen and neon (mainly that of the [O III]λ5007 line, which is 10.3 ± 0.2 times brighter than the Hβ line) therefore reveals the presence of a RE AGN[19]. Bayesian inference of the galaxy's spectral energy distribution (SED; Methods and Fig. 3b) independently suggests the presence of a luminous SMBH accretion disk with an obscuring torus: our model requires these structures to explain the observed infrared (WISE) and near-ultraviolet (Legacy) flux density levels, which exceed those possible with cold dust and stars alone.

By contrast, all previous record-length outflows, such as 3C 236 ($l_p = 4.6$ Mpc (ref. 7)), J1420−0545 ($l_p = 4.9$ Mpc (ref. 8)) and Alcyoneus ($l_p = 5.0$ Mpc (ref. 9)), are fuelled by RI AGN in recent history ($t_{BB} = 10.2$–12.4 Gyr). Whereas RI AGN occur primarily in evolved, 'red and dead' ellipticals[17], RE AGN feature vigorous gas inflows and are thus generally found in star-forming galaxies. Indeed, in the first billions of years of cosmic time, RE AGN dominated the radio-luminous AGN population[20]. The potential of Mpc-scale outflows to spread cosmic rays, heat, heavy atoms and magnetic fields through the IGM is particularly high if large specimina could emerge from the type of AGN abundant at early epochs, when the Universe was smaller. The discovery of a 7-Mpc-long, RE-AGN-fuelled outflow before cosmic half-time therefore highlights the hitherto understudied cosmological transport capabilities of Mpc-scale outflows.

In the Local Universe, about 30% of all luminous Mpc-scale outflows reside in galaxy clusters, about 60% in galaxy groups and the remaining

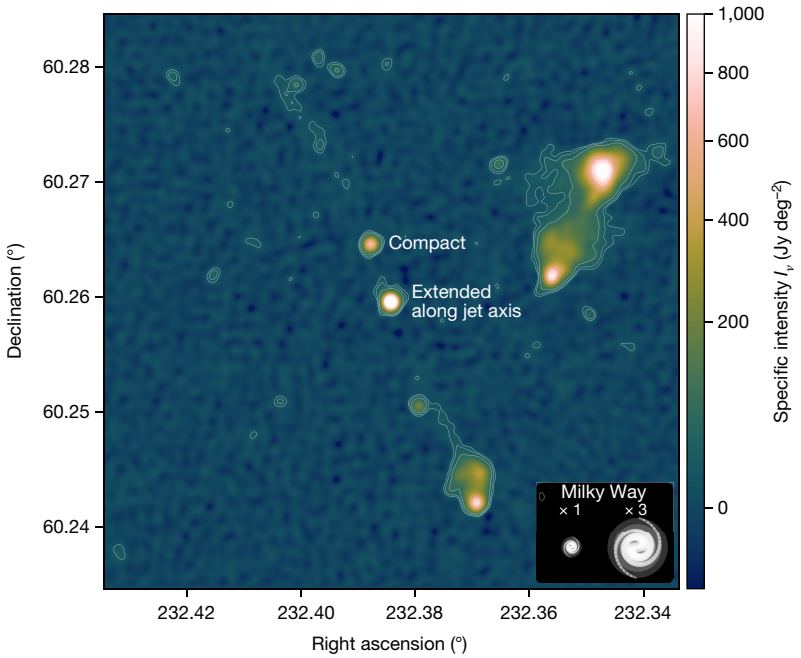

Fig. 2 | Radio close-up of the centre of Porphyrion. In our imagery, only the southern host galaxy candidate features an extension along the overarching jet axis of the outflow. For the central 3′ × 3′ sky area, we show a uGMRT image at $\lambda = 0.46$ m and 3.6″ resolution. We detect the radio extension of the southern galaxy, directed towards the north–northeast, at 5 s.d. (σ) significance. The contours denote 3σ, 5σ, 10σ and 100σ.

roughly 10% in more dilute parts of filaments, in sheets or in voids[21]. The Legacy Surveys DR10 (Fig. 1b inset) suggests that Porphyrion does not originate from a galaxy cluster: the closest known cluster[22] lies at a comoving distance of 30^{+12}_{-17} Mpc , or 31^{+14}_{-16} cluster radii (Methods). The nearest Planck Sunyaev–Zel'dovich detection[23] is about 2° away. Concordantly, studies have found that jet-fuelling RE AGN avoid rich environments[24,25]. In a sphere with a comoving radius of 10 Mpc centred on the host of Porphyrion, we counted 35 ± 6 other Legacy-detected galaxies. By also performing galactic neighbour counts for a control sample of galaxies at comparable redshifts, and by assuming that galactic neighbour counts increase with circumgalactic cosmic web density, we estimated the circumgalactic cosmic web density percentile of Porphyrion to be 42^{+26}_{-23}% (Methods). This suggests that Porphyrion does not originate from a void. The straightness of the outflow implies a low peculiar speed ($v_p \lesssim 10^2$ km s^{-1}), consistent with the host being at the bottom of a local gravitational potential well. The evidence implies that Porphyrion originates from a cosmic web filament, and from a galaxy group in particular. Vast voids, which make up the bulk (about 80%) of the Universe's volume[26], surround such structures in most directions. Jets as long as those of Porphyrion thus encounter void-like densities and temperatures with considerable probability. Indeed, the collimated nature of the jets favours scenarios in which they descend into voids, as jets gain resilience against Kelvin–Helmholtz instabilities when the ambient density declines (for example, ref. 11). Dynamical modelling suggests a two-sided jet power $Q = 1.3 \pm 0.1 \times 10^{39}$ W and an age $T = 1.9^{+0.7}_{-0.2}$ Gyr (Fig. 4; Methods). The average expansion speed of the outflow is $v = 0.012c$, comparable with that of Alcyoneus[9]. In voids and the warm–hot IGM, the speed of sound $c_s \approx 10^0$–10^1 km s^{-1}: the jets grow hypersonically at Mach numbers $\mathcal{M} \approx 10^2 - 10^3$ and drive strong shocks into voids. The jets of Porphyrion have carried an energy $E = QT = 8^{+2}_{-1} \times 10^{55}$ J into the IGM—an amount comparable with the energy released during galaxy cluster mergers (for example, ref. 27). This suggests that the outflow is among the most energetic post-Big Bang events to have occurred in its cosmic web region. Even though the SMBH might have gained a notable fraction of its mass while powering the jets ($\Delta M_\bullet > 2\frac{E}{c^2} = 9^{+2}_{-1} \times 10^8\ M_\odot$), it seems to have maintained a constant spin axis throughout gigayears of activity. Shocks running perpendicular to the jets dissipate enough heat into the filament to increase its temperature by $\Delta T \approx 10^7$ K and its radius by $\Delta r \approx 1$ Mpc (Methods). Outflows such as Porphyrion thus locally alter the shape of the cosmic web.

Figure 4 shows that the radio luminosities of Mpc-long outflows with constant jet power initially decrease before stabilizing to a jet-power-dependent level. Active outflows not only lengthen but also grow volumetrically[15]; consequently, the mean radio luminosity per unit of lobal volume decreases over time. In turn, lobal radio surface brightnesses decrease[21], impeding outflow detection[14,15]. As Fig. 1 shows, Porphyrion borders on the noise of leading current-day telescopes; thus, outflows further progressed on the same evolutionary track hitherto evade detection. Similar outflows are likewise undetectable at lower jet powers and at higher redshifts, at which increased inverse Compton scattering with the cosmic microwave background diverts electron energy away from synchrotron radiation, causing lower radio luminosities at fixed jet powers[28]. Problematically, cosmological surface brightness dimming further reduces radio surface brightnesses by a factor of $(1+z)^{3-\alpha}$, in which α is the radio spectral index. Statistical modelling[14,15] indeed suggests that the detectable population is just the tip of the iceberg: owing to their apparent faintness, most Mpc-scale outflows are still concealed by noise. These arguments, and the fact that our search covered only about 15% of the sky, imply the existence of a hidden population of outflows with sizes comparable with, and possibly larger than, that of Porphyrion.

Porphyrion indicates that RE AGN may be at least as effective at generating Mpc-scale outflows as RI AGN are in the Local Universe. If the comoving number density of actively powered Mpc-scale outflows has remained roughly constant over time at about 10^1 (100 Mpc)$^{-3}$ (refs. 14,15), and a comoving volume of (100 Mpc)^3 contains roughly 10^2 filaments, then there would exist about 10^{-1} actively powered Mpc-scale outflows in every filament at every instant. As their jets endure for approximately 10^{-2}–10^0 Gyr (refs. 1,3,9), approximately 10^1 Mpc-scale outflows may have been generated in every filament throughout cosmic history. If jet powers $Q \approx 10^{38}$ W are typical[1,9,28], Mpc-scale outflows induce substantial heating ($\Delta T \approx 10^6$ K) and expansion ($\Delta r \approx 10^{-1}$ Mpc)

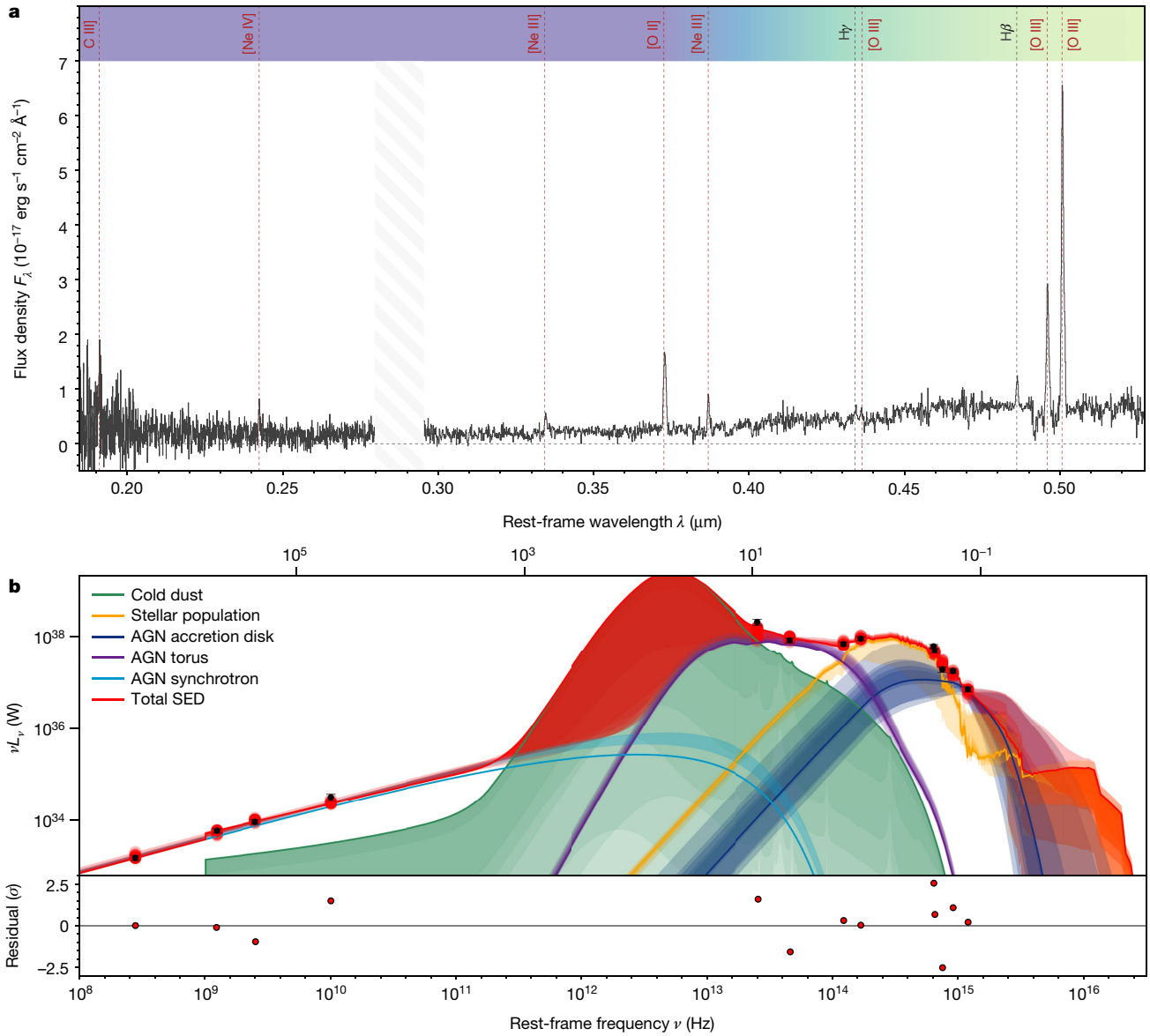

Fig. 3 | Rest-frame ultraviolet–optical spectroscopy and radio–ultraviolet photometry of the host galaxy. Both demonstrate that Porphyrion arises from a RE AGN. **a**, LRIS spectrum exhibiting hydrogen, carbon, oxygen and neon emission. The forbidden lines from multiply ionized oxygen and neon (dark red) could not be generated by even the hottest stars and instead originate from the narrow-line region of a RE AGN at a redshift $z = 0.896 \pm 0.001$. **b**, Bayesian inference of the galaxy's SED (Methods) favours the presence of an AGN accretion disk (dark blue) with an obscuring torus (purple), again indicating radiative efficiency. Residuals are given in multiples of the s.d. (σ).

of cosmic filaments (Methods), which comprise the primary baryon reservoir of the Universe. Whereas AGN feedback has been known to maintain the thermodynamic state in the 1-Mpc^3-scale volumes of galaxy clusters, the discovery of Porphyrion highlights the importance of black hole energy transport in the cosmic web at large.

Online content

Any methods, additional references, Nature Portfolio reporting summaries, source data, extended data, supplementary information, acknowledgements, peer review information; details of author contributions and competing interests; and statements of data and code availability are available at https://doi.org/10.1038/s41586-024-07879-y.

1. Hardcastle, M. J. et al. Radio-loud AGN in the first LoTSS data release. The lifetimes and environmental impact of jet-driven sources. *Astron. Astrophys.* **622**, A12 (2019).
2. Perucho, M., Martí, J.-M. & Quilis, V. Long-term FRII jet evolution: clues from three-dimensional simulations. *Mon. Not. R. Astron. Soc.* **482**, 3718–3735 (2019).
3. Dabhade, P., Saikia, D. J. & Mahato, M. Decoding the giant extragalactic radio sources. *J. Astrophys. Astron.* **44**, 13 (2023).
4. Ayromlou, M., Nelson, D. & Pillepich, A. Feedback reshapes the baryon distribution within haloes, in halo outskirts, and beyond: the closure radius from dwarfs to massive clusters. *Mon. Not. R. Astron. Soc.* **524**, 5391–5410 (2023).
5. Beck, A. M., Hanasz, M., Lesch, H., Remus, R. S. & Stasyszyn, F. A. On the magnetic fields in voids. *Mon. Not. R. Astron. Soc.* **429**, L60–L64 (2013).
6. Vazza, F. et al. Simulations of extragalactic magnetic fields and of their observables. *Class. Quantum Gravity* **34**, 234001 (2017).
7. Willis, A. G., Strom, R. G. & Wilson, A. S. 3C236, DA240; the largest radio sources known. *Nature* **250**, 625–630 (1974).
8. Machalski, J., Kozieł-Wierzbowska, D., Jamrozy, M. & Saikia, D. J. J1420–0545: the radio galaxy larger than 3C 236. *Astrophys. J.* **679**, 149–155 (2008).
9. Oei, M. S. S. L. et al. The discovery of a radio galaxy of at least 5 Mpc. *Astron. Astrophys.* **660**, A2 (2022).
10. Correa, C. M. et al. Redshift-space effects in voids and their impact on cosmological tests. Part I: the void size function. *Mon. Not. R. Astron. Soc.* **500**, 911–925 (2021).
11. Perucho, M. Dissipative processes and their role in the evolution of radio galaxies. *Galaxies* **7**, 70 (2019).
12. Andernach, H., Jiménez-Andrade, E. F. & Willis, A. G. Discovery of 178 giant radio galaxies in 1059 deg^2 of the Rapid ASKAP Continuum Survey at 888 MHz. *Galaxies* **9**, 99 (2021).

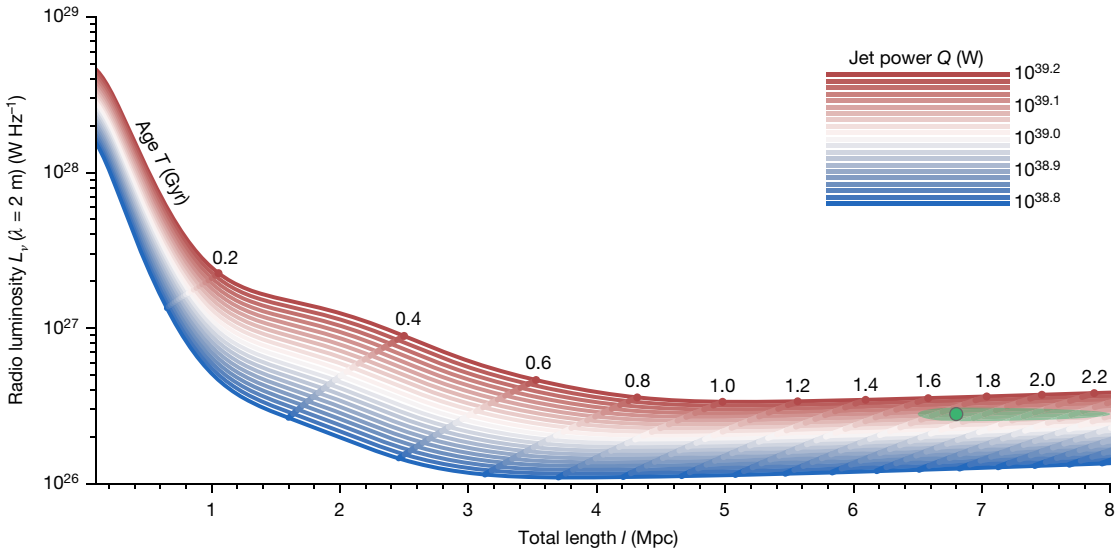

Fig. 4 | Measurements overlaid on evolutionary tracks from dynamical modelling. By superimposing the total length and radio luminosity of Porphyrion on these tracks, we inferred the two-sided jet power and age of the outflow. We assumed the host galaxy to reside in a galaxy group bordering voids, through which the jets eventually travel. The width and height of Porphyrion's uncertainty ellipse both cover 68% of probability centred on the median (green dot).

13. Dabhade, P. et al. Giant radio galaxies in the LOFAR Two-metre Sky Survey. I. Radio and environmental properties. *Astron. Astrophys.* **635**, A5 (2020).
14. Oei, M. S. S. L. et al. Measuring the giant radio galaxy length distribution with the LoTSS. *Astron. Astrophys.* **672**, A163 (2023).
15. Mostert, R. I. J. et al. Constraining the giant radio galaxy population with machine learning and Bayesian inference. Preprint at https://arxiv.org/abs/2405.00232 (2024).
16. Hardcastle, M. J. et al. The LOFAR Two-Metre Sky Survey. VI. Optical identifications for the second data release. *Astron. Astrophys.* **678**, A151 (2023).
17. Heckman, T. M. & Best, P. N. The coevolution of galaxies and supermassive black holes: insights from surveys of the contemporary universe. *Annu. Rev. Astron. Astrophys.* **52**, 589–660 (2014).
18. Hardcastle, M. Interpreting radiative efficiency in radio-loud AGNs. *Na. Astron.* **2**, 273–274 (2018).
19. Buttiglione, S. et al. An optical spectroscopic survey of the 3CR sample of radio galaxies with $z < 0.3$. II. Spectroscopic classes and accretion modes in radio-loud AGN. *Astron. Astrophys.* **509**, A6 (2010).
20. Williams, W. L. et al. LOFAR-Boötes: properties of high- and low-excitation radio galaxies at $0.5 < z < 2.0$. *Mon. Not. R. Astron. Soc.* **475**, 3429–3452 (2018).
21. Oei, M. S. S. L. et al. Luminous giants populate the dense Cosmic Web. The radio luminosity–environmental density relation for radio galaxies in action. *Astron. Astrophys.* **686**, A137 (2024).
22. Wen, Z. L. & Han, J. L. A catalog of 1.58 million clusters of galaxies identified from the DESI Legacy Imaging Surveys. *Astrophys. J. Suppl. Ser.* **272**, 39 (2024).
23. Planck Collaboration et al. Planck 2015 results. XXVII. The second Planck catalogue of Sunyaev-Zeldovich sources. *Astron. Astrophys.* **594**, A27 (2016).
24. Ineson, J. et al. Radio-loud active galactic nucleus: is there a link between luminosity and cluster environment? *Astrophys. J.* **770**, 136 (2013).
25. Ineson, J. et al. The link between accretion mode and environment in radio-loud active galaxies. *Mon. Not. R. Astron. Soc.* **453**, 2682–2706 (2015).
26. Forero-Romero, J. E., Hoffman, Y., Gottlöber, S., Klypin, A. & Yepes, G. A dynamical classification of the cosmic web. *Mon. Not. R. Astron. Soc.* **396**, 1815–1824 (2009).
27. van Weeren, R. J. et al. Radio observations of ZwCl 2341.1+0000: a double radio relic cluster. *Astron. Astrophys.* **506**, 1083–1094 (2009).
28. Hardcastle, M. J. A simulation-based analytic model of radio galaxies. *Mon. Not. R. Astron. Soc.* **475**, 2768–2786 (2018).

Methods

Throughout this work, we assume a flat, inflationary ΛCDM cosmological model with parameters from ref. 29: $h = 0.6766$, $\Omega_{\mathrm{BM},0} = 0.0490$, $\Omega_{\mathrm{M},0} = 0.3111$ and $\Omega_{\Lambda,0} = 0.6889$. We define $\Omega_{\mathrm{DM},0}$ as $\Omega_{\mathrm{M},0} - \Omega_{\mathrm{BM},0} = 0.2621$ and H_0 as $h \times 100\ \mathrm{km\ s^{-1}\ Mpc^{-1}}$. Furthermore, we define the spectral index α so that it relates to flux density F_ν at frequency ν as $F_\nu \propto \nu^\alpha$. Under this convention, synchrotron spectral indices are positive (that is, $\alpha = \frac{5}{2}$) for the lowest frequencies and negative for higher frequencies. As the restoring point spread functions may not be perfectly circular, all reported resolutions are effective resolutions. In other works, Mpc-scale outflows are usually called 'giant radio galaxies'. (Although Mpc-scale outflows are generated by galaxies, they are not galaxies themselves; therefore, referring to them as a class of 'galaxies' could cause confusion. Also, Mpc-scale outflows may have been primarily studied through radio observations, but their synchrotron losses (such as their other radiative losses) seem to have only a minor effect on their evolution[28], suggesting that 'radio' should not be used in a name meant to describe these objects intrinsically. Finally, although 'giant' seems apt, it is also vague; we thus prefer the more quantitative term 'Mpc-scale').

ILT observations and data reduction

The ILT[30] is very sensitive to the metre-wavelength synchrotron radiation generated by electrons and positrons in the first tens to hundreds of megayears after their acceleration to relativistic energies. Consequently, the second data release (DR2; ref. 31) of the LOFAR Two-metre Sky Survey (LoTSS; ref. 32), the ILT's continuing northern sky survey in the 120–168-MHz frequency band, has revealed millions of galaxies boasting SMBH jets.

After discovering Porphyrion, the outflow presented in this work, we extracted a total of 16 h of DDFacet-calibrated visibilities[33] from LoTSS pointings P228+60 and P233+60 (project ID: LT5_007). (Porphyrion was the son of Ouranos, the Greek primordial sky deity. According to Pseudo-Apollodorus, he and Alcyoneus were the greatest of the Gigantes (Giants), whereas Pindar called him the 'king of the Giants'. He was struck by Zeus's thunderbolt in the Gigantomachy—the battle between the Giants and the Olympian gods for supremacy over the Cosmos.) Following ref. 34, we subtracted all sources far away from the target, performed phase shifting and averaging and self-calibrated the resulting data. This removed residual ionospheric artefacts around ILT J153004.28+602423.2, the brightest source in the arcminute-scale vicinity of the northern lobe. We subsequently performed joint deconvolution on the recalibrated target visibilities with WSClean[35] using Briggs weighting −0.5, yielding the 6.2″-resolution image of Fig. 1a. The noise level is $\sigma = 25\ \mathrm{Jy\ deg^{-2}}$ at its lowest. The outflow seems thin: its width is nowhere more than a few percent of its length. We defined the angular length of Porphyrion as the largest possible great-circle distance between a point in the southernmost hotspot and a point in the northern lobe. The arc connecting these points defines the overarching jet axis and we measured its position angle to be 27 ± 1°.

To investigate the presence of diffuse structure, we applied Gaussian tapering to the weights of the recalibrated target visibilities. The full width at half maximum (FWHM) of the taper in the (u, v) plane was chosen such that the FWHM of the corresponding Gaussian in the sky plane equals 15″. Again, performing deconvolution with WSClean using Briggs weighting −0.5 (albeit in multiscale mode this time), we obtained the 19.8″-resolution image of Extended Data Fig. 1. This image reveals the northern lobe more clearly. The noise level is $\sigma = 4.8\ \mathrm{Jy\ deg^{-2}}$.

To obtain a high-resolution image of Porphyrion, we reprocessed the P233+60 data, including LOFAR's international stations, from scratch using the LOFAR-VLBI pipeline[36]. This pipeline builds on the calibration pipeline for the Dutch part of the array to calibrate the international stations. We derived the dispersive phase corrections and gain corrections for the international stations by calibrating against a bright and compact radio source near the target. In this case, we used the aforementioned ILT J153004.28+602423.2, a known source from the Long-Baseline Calibrator Survey (LBCS; refs. 37,38). To reduce interference from unrelated radio sources in the angular vicinity of Porphyrion, we phased up the core stations of LOFAR to narrow down the field of view and only considered data from long baselines to calculate the calibration solutions. With the calibration solutions applied in the direction of the target, we again performed deconvolution with WSClean (but using Briggs weighting 0) to obtain a 0.4″-resolution image, which we show partially in Fig. 1a inset and fully in Extended Data Fig. 2. The noise level is $\sigma = 2.7 \times 10^3\ \mathrm{Jy\ deg^{-2}}$ at its lowest. This image, which covers the central one-third of the total jet system, reveals synchrotron emission at 42σ significance from AGN in only two galaxies, 19″ apart. Both lie along the jet axis of the outflow nearly halfway between its end points. We considered these galaxies, J152933.03+601552.5 and J152932.16+601534.4, to be the host candidates of Porphyrion. In contrast to other radio-emitting structures along the jet axis, such as the southern complex interpreted as an inner hotspot, these candidates have optical counterparts in Legacy Surveys DR10 imagery (Fig. 1b inset).

uGMRT observations and data reduction

On 13 May 2023, we observed the outflow with the uGMRT[39] in Band 4 (550–750 MHz) for a total of 10 h. On 23 September 2023, we extended these observations with another 5 h. These observations are part of GMRT Observing Cycle 44 and have project code 44_101. We requested to record both narrow-band (GSB) and wide-band (GWB) data. Adverse ionospheric conditions during the September run prohibited us from improving on the images produced with the May run data only. In what follows, we therefore exclusively discuss May run data reduction and results. We performed calibration with Source Peeling and Atmospheric Modeling (SPAM; ref. 40), starting with the GSB data. After direction-dependent calibration, we used Python Blob Detection and Source Finder (PyBDSF; ref. 41) to derive a sky model from the final GSB image, which subsequently served to initialize the direction-dependent calibration of the GWB data. As SPAM was designed with narrow-band data in mind, following standard practice, we first split the GWB data along the frequency axis, yielding four subbands of 50 MHz width each. We then calibrated each subband independently. A joint image of four calibrated subbands revealed residual ionospheric artefacts from ILT J153004.28+602423.2, the same bright source in the vicinity of the northern lobe mentioned earlier. To mitigate these artefacts, we subtracted (on a subband basis) all sources outside a spherical cap with a 9′ radius centred on J2000 right ascension $\varphi = 15\ \mathrm{h}\ 29\ \mathrm{min}\ 32.0\ \mathrm{s}$ and declination $\theta = 60°\ 15'\ 33.0''$. We then jointly reimaged the four source-subtracted subbands with WSClean, using Briggs weighting 0. This resulted in the 4.3″-resolution image of Fig. 1b. The noise level is $\sigma = 3\ \mathrm{Jy\ deg^{-2}}$ at its lowest.

In the Legacy Surveys DR10 optical imagery shown in Fig. 1b inset, we identified two faint galaxies in the arcsecond-scale vicinity of the southern host galaxy candidate. Of these, the galaxy at $(\varphi, \theta) = (232.37969°, 60.26029°)$ emits low-frequency radio emission at 6σ significance. At the 4.3″ resolution of our fiducial uGMRT image, this radio emission is only narrowly separable from that of the host galaxy candidate, thus interfering with establishing the radio morphology of the candidate. Trading depth for resolution, we reimaged the uGMRT data with WSClean using Briggs weighting −0.5, yielding a 3.6″ resolution. Subsequently, to isolate the radio morphology of J152932.16+601534.4, we fit a circular Gaussian fixed at the sky coordinates of its radio-emitting neighbour. Naturally, we set the FWHM of this Gaussian to 3.6″. On subtracting the Gaussian, we obtained our final image; Fig. 2 shows its central region, in which the noise level is $\sigma = 6\ \mathrm{Jy\ deg^{-2}}$ at its lowest. Only the southern (and most radio-luminous) host galaxy candidate features an extension along the overarching jet axis seen in Fig. 1. (Radio luminosity L_ν is, at fixed redshift and large-scale halo mass, approximately proportional to jet power Q (ref. 28). Under the Blandford–Znajek mechanism[42], $Q \propto M_\bullet^2$ (at fixed magnetic field strength and spin), in

which $M_\bullet$ is the SMBH mass. As the generation of Porphyrion's jets entails a marked SMBH mass gain $\Delta M_\bullet \approx 10^8$–$10^9\,M_\odot$, the SMBH must now be massive; hence, a high radio luminosity is expected). In our data, this extension—indicative of a pair of relativistically beamed jets—occurs at 5σ significance.

We estimated the probability to find a spurious (that is, unrelated) radio-luminous AGN (RLAGN) with jets along the overarching axis of Porphyrion in the region in which the host galaxy could plausibly reside. To find the sky density of RLAGN with discernible jet orientations at arcsecond-scale resolutions, metre-scale wavelengths and 10^1 Jy deg^{-2}-scale noise levels, we studied the LoTSS DR1-derived RLAGN sample presented in ref. 1. This sample, consisting of 23,344 RLAGN, contains 6,850 RLAGN with discernible jet orientations. The latter population's average sky density $\bar{n}_s = 4 \times 10^{-3}$ arcmin^{-2}. Approximating the sky density n_s of spurious RLAGN with discernible jet orientations near the host of Porphyrion with $\bar{n}_s$ would be appropriate only if such RLAGN would not cluster in the sky. Optimally, we estimated n_s by first counting, for each such RLAGN (that seems sufficiently far from the edges of the survey footprint), the number of neighbours in disks of radius 1′. Next, we divided each count by the solid angle of the disks and, finally, determined the sample mean: $n_s = 8 \times 10^{-3}$ arcmin^{-2}. (For disks of larger radii, n_s approaches $\bar{n}_s$). We estimated the solid angle of the 'strip' in which an unrelated source could be mistaken for the host of Porphyrion to be $\Omega_s = 10^0 \times 10^{-1}$ arcmin^2. (We limited the angular length of the strip by asserting that plausible host candidates lie between Porphyrion's two detected patches of jet emission). Defining jets 'aligned' with those of Porphyrion when their position angle falls within a range of width 10^1 deg centred on the position angle of Porphyrion, the probability of randomly attaining alignment $p_s = \frac{10^\circ}{180^\circ} = 6 \times 10^{-2}$. One thus expects to encounter $\mathbb{E}[N_s] = n_s \times \Omega_s \times p_s = 4 \times 10^{-5}$ unrelated RLAGN with resolved and aligned jets near the host of Porphyrion. Assuming that N_s is Poisson-distributed, one or more such spurious sources appear with a probability $\mathbb{P}(N_s \geq 1) = 1 - e^{-\mathbb{E}[N_s]} \approx \mathbb{E}[N_s]$. (This approximation improves as $\mathbb{E}[N_s]$ decreases). We thus find $\mathbb{P}(N_s \geq 1) = 4 \times 10^{-5}$; the probability to find a spurious unresolved RLAGN in the same region is 4×10^1 times larger. We conclude that J152932.16+601534.4 is the host galaxy of Porphyrion.

Keck I observations and data reduction

The literature offers only photometric redshift estimates of the host galaxy. The SDSS DR12 (ref. 43) reports $z_p = 0.68 \pm 0.06$, the Legacy Surveys DR9 (ref. 44) reports $z_p = 0.93 \pm 0.08$ and ref. 45 reports $z_p = 0.92 \pm 0.08$. For radio-emitting galaxies such as J152932.16+601534.4, we consider the last estimate to be most reliable.

To establish the redshift of Porphyrion's host galaxy with certainty, we measured its (rest-frame) ultraviolet–optical spectrum with the LRIS[46–49] on the W. M. Keck Observatory's Keck I telescope. Adequate slit placement requires accurate knowledge of the galaxy's coordinates. From the Legacy Surveys DR10 best-fit model, we found that the centre of J152932.16+601534.4 lies at $(\varphi, \theta) = (232.38410^\circ, 60.25960^\circ)$. The half-light radius of the galaxy is 10.1 ± 0.3 kpc. On 23 June 2023, we observed the galaxy for a total of 900 s. We used the 600/4000 grism on the blue side of LRIS, with 1×2 binning (spatial and spectral, respectively), and the 400/8500 grating on the red side, again with 1×2 binning. During the observations, the seeing was approximately 0.8″; as we used a 1.5″ slit, minimal slit losses occurred. Using a slit position angle of −70°, we could simultaneously obtain a spectrum for J152933.03+601552.5, the quasar-hosting galaxy that we initially considered (and then discarded) as a host candidate. We reduced the data with PypeIt[50], a Python-based pipeline with features tailored to reducing LRIS long-slit spectroscopy. We flat-fielded and sky-subtracted the data using standard techniques. We used internal arc lamps for wavelength calibration and a standard star for overall flux calibration.

The final LRIS-derived spectra of J152932.16+601534.4 and J152933.03+601552.5 are shown in Fig. 3 and Extended Data Fig. 3, respectively. The corresponding spectroscopic redshifts are $z_s = 0.896 \pm 0.001$ and $z_s = 0.799 \pm 0.001$. The uncertainties reflect the limited spectral resolution of the LRIS, as well as systematic errors in wavelength calibration. The latter spectroscopic redshift can be compared with the value derived for J152933.03+601552.5 by the SDSS BOSS[51] on 5 July 2013. Visual inspection of the SDSS BOSS spectrum and its best fit indicates a robust spectroscopic redshift $z_s = 0.79836 \pm 5 \times 10^{-5}$. The two measurements are in agreement.

SED

To further assess the accretion mode of Porphyrion's AGN and to estimcate its host's stellar mass and possibly star formation rate (SFR), we performed SED inference. Through VizieR, the Astro Data Lab and the NASA/IPAC Extragalactic Database, we collected catalogued total (rather than fixed-aperture) flux densities, relative flux densities, magnitudes, galactic transmission fractions and total extinctions from rest-frame ultraviolet to radio wavelengths. Extended Data Fig. 4 shows the cross-matching results. It demonstrates that the host galaxy of Porphyrion (as identified in Legacy Surveys DR10) is, in view of the astrometric accuracies of the collected catalogue data, the only plausible match. Just 2.7″ northeast from the host galaxy of Porphyrion lays another source, which could be either a Milky Way star or a galaxy. Mindful of the possibility of spuriously high flux density measurements as a result of target–neighbour blending, we assessed all images underlying the catalogued estimates by eye. The neighbouring source only seems to be a point of attention for flux density measurements at small wavelengths, such as in the Legacy *g*-band and *r*-band, in which it has flux densities about 100% and about 60% those of the target, respectively. At the larger wavelengths of the Legacy *z*-band, the flux density of the neighbour is small (roughly 20%) relative to that of the target. The error induced by blending, which will add only a fraction of the neighbour's flux density, should thus be negligible. Accordingly, the Pan-STARRS and WISE measurements at even larger wavelengths are not compromised by this neighbour.

We converted the Legacy relative flux densities to flux densities by multiplying with the reference flux density $F_\nu = 3{,}631$ Jy. We converted the Pan-STARRS AB magnitudes to flux densities using the standard relation (for example, equation (1) of ref. 52). We converted the WISE relative flux densities to flux densities by multiplying with the reference flux densities in Table 1 of ref. 53. Extended Data Table 1 provides all retained flux densities F_ν and the central wavelengths λ to which they correspond.

The host galaxy of Porphyrion lies at a galactic latitude $b = 47.43194^\circ$. Fortunately, at these latitudes, the galactic transmission is high for all bands included in our SED inference. We tabulate estimated transmitted fractions f_t in Extended Data Table 1. For Pan-STARRS *i* and *y*, we calculated f_t from total extinctions $A_\lambda = 0.022$ and $A_\lambda = 0.014$, respectively, using $f_t = 10^{-\frac{2}{5}A_\lambda}$. For Legacy *g*, in which galactic transmission is lowest, application of the correction factor f_t^{-1} results in a flux density increase of just 4%. For all bands, the correction is smaller than the flux density uncertainty. We conclude that, for our purposes, galactic extinction can be neglected.

Next, using AGNfitter[54,55], we determined the SED posterior shown in Fig. 3b. The posterior indicates the presence of a luminous SMBH accretion disk with an obscuring torus, confirming the RE nature of Porphyrion's AGN. The SED posterior further implies that the stellar mass of Porphyrion's host is $M_\star = 6.7 \pm 1.4 \times 10^{11}\,M_\odot$. To gauge the sensitivity of stellar mass estimates for this galaxy to methodological variation, we compare our result with the corresponding stellar mass estimate in the LoTSS DR2 value-added catalogue[16]. The authors of this catalogue derive a stellar mass $M_\star = 5.5^{+0.7}_{-0.6} \times 10^{11}\,M_\odot$ from SED fits to Legacy *g*, *r*, *z* and WISE W1 and W2 flux densities. (This stellar mass estimate is not based on the spectroscopic redshift we have obtained through the LRIS but uses a photometry-based redshift posterior with mean and standard deviation $z_p = 0.92 \pm 0.08$ (ref. 45)). The two stellar

mass measurements are in agreement. Owing to the lack of rest-frame far-infrared photometry, the SFR of Porphyrion's host is virtually unconstrained by the SED posterior.

Radio luminosities and spectral indices

To determine metre-wavelength radio luminosities and a metre-wavelength spectral index for Porphyrion, we first measured its flux densities in the 6.2″ ILT and 4.3″ uGMRT images. We assumed flux scale uncertainties of 10% and 5%, respectively.

Summing over all structural components, the total flux density of the outflow at $\lambda = 2.08$ m is $F_\nu = 63 \pm 6$ mJy. Its total radio luminosity at rest-frame wavelength $\lambda_r = 1.10$ m is therefore $L_\nu = 1.4 \pm 0.1 \times 10^{26}$ W Hz^{-1}; the core radio luminosity, $L_\nu = 5.3 \pm 0.5 \times 10^{24}$ W Hz^{-1}, comprises about 4% of the total. The total flux density of the outflow at $\lambda = 0.46$ m is $F_\nu = 12.0 \pm 0.6$ mJy. Its total radio luminosity at $\lambda_r = 0.24$ m is therefore $L_\nu = 2.7 \pm 0.1 \times 10^{25}$ W Hz^{-1}; the core radio luminosity, $L_\nu = 4.7 \pm 0.2 \times 10^{24}$ W Hz^{-1}, comprises about 17% of the total. These data imply a metre-wavelength total spectral index $\alpha = -1.09 \pm 0.08$ and a core spectral index $\alpha = -0.09^{+0.08}_{-0.07}$. Through spectral-index-based interpolation, we estimated the total radio luminosity at $\lambda_r = 2$ m to be $L_\nu = 2.8 \pm 0.3 \times 10^{26}$ W Hz^{-1}. This latter total radio luminosity is an important input for our dynamical modelling.

We calculated directionally resolved metre-wavelength spectral indices by combining the ILT and uGMRT images. Before doing so, we convolved the latter image to the resolution of the former. In Extended Data Fig. 5, we show two regions of interest from the resulting spectral index map, which consequently has a resolution of 6.2″. To highlight the directions in which our spectral index measurements are informative, we blanked all directions in which the thermal-noise-induced spectral index uncertainty exceeds 0.3. The top panel of Extended Data Fig. 5 shows that J152932.16+601534.4, the host galaxy of Porphyrion, has a much higher spectral index than J152933.03+601552.5, the aforementioned quasar-hosting galaxy. The former spectral index is consistent with zero, indicating that the onset of synchrotron self-absorption (SSA) in the host galaxy of Porphyrion occurs at metre wavelengths. By contrast, the onset of SSA in the quasar-hosting galaxy must occur at longer wavelengths, suggesting a lower lepton energy density and weaker magnetic fields in its synchrotron-radiating region. The bottom panel of Extended Data Fig. 5 shows that the southern tip of Porphyrion features much lower spectral indices, with a gradient along the jet axis. This gradient is consistent with a scenario of a hotspot with backflow in which spectral ageing occurs. Whereas $\alpha = -1.0 \pm 0.2$ at the southwestern side of the hotspot, the radio spectra gradually steepen to $\alpha = -1.6 \pm 0.2$ at the northeastern side of the hotspot. No spectral trend seems to be present further downstream.

We investigated more thoroughly whether the metre-wavelength spectral index discrepancy between J152932.16+601534.4 and J152933.03+601552.5 constitutes evidence that the former galaxy is the host of Porphyrion. For each of the 1.1×10^4 Mpc-scale outflows catalogued in ref. 15, we sought to determine LoTSS DR2 and VLASS core flux densities. LoTSS DR2 core flux densities were available for 1,238 Mpc-scale outflows, whereas VLASS core flux densities were available for 6,882. We found 924 Mpc-scale outflows for which both core flux densities were available; for these, we computed 144 MHz to 3 GHz spectral indices. Extended Data Fig. 6 summarizes the results. The sample mean and standard deviation are −0.25 and 0.33, respectively; the median is −0.24 and 68% of all spectral indices lie between −0.58 and 0.09. It is likely that some VLASS-detected cores are undetectable in the LoTSS DR2 because of a combination of low VLASS flux densities and flat ($\alpha \simeq 0$) or 'inverted' ($\alpha > 0$) radio spectra. The consequence is a bias in Extended Data Fig. 6 towards lower spectral indices. By requiring that the LoTSS DR2 core is an isolated source on the sky, the core spectral indices of Fanaroff–Riley (FR) I outflows have probably been selected out. As Porphyrion is a FR II outflow, deselecting FR I outflows may have the beneficial effect of making the distribution more representative of the object under study here. As shown in Extended Data Fig. 6 inset, the spectral indices in this sample do not exhibit a strong trend with redshift. Consequently, no marked distributional changes occurred when we restricted the sample to the 254 Mpc-scale outflows whose redshifts differ at most $\Delta z = 0.1$ from those of either J152932.16+601534.4 or J152933.03+601552.5 (orange histogram in Extended Data Fig. 6). We conclude that the known core spectral indices of Mpc-scale outflows favour J152932.16+601534.4 over J152933.03+601552.5 as the host of Porphyrion, strengthening our earlier identification.

Cosmic web environment

Cosmic web environment characterizations of luminous ($L_\nu(\nu = 150\ \mathrm{MHz}) \geq 10^{24}$ W Hz^{-1}) Mpc-scale outflows in the Local Universe ($z \lesssim 0.2$) have recently been obtained[21] by localization in Bayesian large-scale structure reconstructions and by cross-matching with catalogues of galaxy clusters ($M_{500} \geq 0.6 \times 10^{14}\ M_\odot$) and galaxy groups ($M_{500} < 0.6 \times 10^{14}\ M_\odot$). The resulting probability distribution over cosmic web environments serves as a prior distribution for Porphyrion's cosmic web environment. In the Local Universe, about 30% of all luminous Mpc-scale outflows reside in clusters, about 60% in groups and the remaining roughly 10% in more dilute parts of filaments, in sheets or in voids[21]. Thus, if this probability distribution does not evolve with redshift and a cluster environment can be excluded, Porphyrion probably originates from a filament. To evaluate whether the host galaxy of Porphyrion inhabits a cluster, we extracted right ascensions, declinations, redshifts and R_{500} radii from the cluster catalogue of Wen and Han[22], which is based on Legacy Surveys DR10. Even though these data allow for cluster detections up to $z \approx 1.5$, we did not find a cluster close to the host of Porphyrion. To reach this conclusion statistically, we first estimated cluster redshift uncertainties using $\sigma_z(z) = 0.02 \times \frac{z}{0.9} \times (1+z)$ for photometric cluster redshifts, as suggested by the bottom-right panel of Fig. 7 of Wen and Han[22], and $\sigma_z = 0.001$ for spectroscopic cluster redshifts. We neglected uncertainties in cluster right ascensions and declinations. We then Monte-Carlo-simulated a redshift for both the host of Porphyrion and all clusters (assuming Gaussian redshift distributions), converted right ascensions, declinations and redshifts into comoving coordinates, and finally identified the cluster nearest to the host of Porphyrion. We recorded the comoving distance to this cluster, as well as the ratio between the corresponding proper distance and the R_{500} radius of the cluster. We repeated this Monte Carlo procedure millions of times, until the probability distributions over these distance measures converged. The results are shown in Extended Data Fig. 7. Around the redshift of Porphyrion, the Wen and Han[22] photometric cluster redshift uncertainties $\sigma_z \approx 0.04$, large enough to force us to consider several clusters as candidates for being the nearest. Each peak corresponds to the smallest possible distance to a possibly nearest cluster. The peak location is determined by both the angle between the host of Porphyrion and the cluster and by the redshift of Porphyrion. In Monte Carlo realizations such that the cluster redshift matches that of Porphyrion, the distance is minimal. The nearest cluster lies at a comoving distance of 30^{+12}_{-17} Mpc, or 31^{+14}_{-16} cluster radii (68% probability intervals); the nearest cluster lies at a comoving distance of 30^{+14}_{-22} Mpc, or 31^{+19}_{-23} cluster radii (95% probability intervals). In just 0.1% of all realizations, the host of Porphyrion host is five or fewer R_{500} radii away from the nearest cluster.

To investigate whether a filament or a void environment is more probable, we performed probabilistic galaxy counts using the Legacy data underlying the Wen and Han[22] cluster catalogue. We extracted right ascensions, declinations, redshift posterior means and redshift posterior standard deviations of all Legacy-detected galaxies that lie within 1.5° of Porphyrion's host. In a similar spirit as before, we then Monte-Carlo-simulated redshifts (in which, for simplicity, we approximated the redshift posterior distributions of galaxies with Gaussian distributions), converted right ascensions, declinations and redshifts into comoving coordinates and counted the number of Legacy-detected

galaxies (excluding the host of Porphyrion) within a sphere of given radius centred on the host of Porphyrion. To properly take into account galactic redshift uncertainties, we repeated this Monte Carlo procedure 1,000 times. In a sphere with a comoving radius of 10 Mpc centred on the host of Porphyrion, we counted 35 ± 6 other Legacy-detected galaxies. We then performed analogous probabilistic galactic neighbour counts for a control sample of galaxies at comparable redshifts. We selected controls by demanding that their redshift means do not deviate more than 0.05 from that of Porphyrion. To ensure that these mean redshifts are reliable, we further demanded that the redshift standard deviations of controls are less than 0.1. From the available candidate controls, we picked 100 controls at random and performed the counts for them. The galactic neighbour count of Porphyrion, relative to those of the control sample, occurs at percentile $42^{+26}_{-23}\%$. If we assume that circumgalactic cosmic web density is a monotonic function of the number of galactic neighbours, the circumgalactic cosmic web density percentile of Porphyrion will be $42^{+26}_{-23}\%$ as well. This suggests that Porphyrion does not originate from a void. In line with the expectation for luminous Mpc-scale outflows in the Local Universe, we conclude that Porphyrion most probably originates from a filament.

Dynamical modelling: jet power and age

We derived the jet power and age of Porphyrion from its length, radio luminosity, cosmological redshift and probable environment by fitting evolutionary tracks. We generated these evolutionary tracks with the simulation-based analytic outflow model in ref. 28. This model requires assumptions on the large-scale environment in which the dynamics take place. Following the previous section, we suppose that the host galaxy resides in the centre of a galaxy group of mass $M_{500} = 10^{13}\,M_\odot$ (which comprises contributions from both dark and baryonic matter)[21,56]. We assigned the group a universal pressure profile (UPP; ref. 57) $p_g(r)$, which can be parametrized just by M_{500}. (Sun et al.[58] have shown that the UPP applies to galaxy groups, even though the profile has originally been proposed to fit data on galaxy clusters—which have much higher masses: $10^{14}\,M_\odot < M_{500} < 10^{15}\,M_\odot$). To obtain the baryon density profile of the group from its pressure profile, we invoked the ideal gas law: $\rho_g(r) = \frac{p_g(r)\langle m\rangle}{k_B T_g}$, in which $\langle m\rangle$ is the average plasma particle mass and T_g the group temperature. We assumed a pure ^{1}H–^{4}He plasma with a ^{4}He mass fraction $Y = 25\%$ (for example, ref. 59), so that $\langle m\rangle \approx \frac{4}{8-5Y} m_p = 0.6 m_p$, in which m_p is the proton mass. We estimated T_g, which we assumed to be constant in space and time, using the mass–temperature relation specified by equation (9) and Tables 3 and 4 in ref. 60:

$$\frac{k_B T_g}{2\ \mathrm{keV}} = 0.77 \times \left(\frac{M_{500}}{5\times 10^{13}\ h_{70}^{-1}\ M_\odot}\right)^{0.61}. \quad (1)$$

The aforementioned mass implies $T_g = 7\times 10^6$ K. As Mpc-scale outflows reach beyond the edges of groups, it was also necessary to estimate the pressure and baryon density in the more distant surroundings of the AGN. Following the bottom-right panel of Fig. 6 in ref. 61, we set the baryon overdensity within voids at the redshift of Porphyrion to $\delta = -0.7$. (In doing so, we implicitly assumed that the baryonic matter overdensity field is identical to the total matter overdensity field—which comprises contributions from both dark and baryonic matter—as ref. 61 considers the latter). We obtained a void baryon density $\rho_v = \rho_{c,0}\Omega_{BM,0}(1+z)^3(1+\delta) = 9\times 10^{-31}$ g cm^{-3}, in which $\rho_{c,0}$ is today's critical density. Following the detailed study of IGM temperatures through cosmic time in ref. 62, which suggests a void temperature $T_v \approx 10^3$–10^4 K at the redshift of Porphyrion, we set $T_v = 1\times 10^4$ K. This choice reflects the fact that we are interested in void temperatures near the galaxy group. Again applying the ideal gas law and taking $\langle m\rangle$ as before, we obtained a void pressure $p_v = 1\times 10^{-19}$ Pa. Finally, we defined the external pressure $p_e(r) = p_g(r) + p_v$, baryon density $\rho_e(r) = \rho_g(r) + \rho_v$ and baryon-density-weighted temperature $T_e(r) = \frac{\rho_g(r)T_g + \rho_v T_v}{\rho_e(r)}$. Extended Data Fig. 8 shows these profiles.

We explored whether the addition of a filament component would substantially change the profiles in Extended Data Fig. 8. We assumed a baryon overdensity $\delta = 10$ at the filament spine and baryon density and temperature profiles following the results in ref. 63 for massive filaments in the EAGLE simulation. We found pressure and baryon density contributions of an importance similar to or less than that of the group, even at Mpc-scale distances. We thus considered the addition of the filament unnecessary, especially in light of model uncertainties such as the mass of the group and the surmised validity of extrapolating the UPP of the group to Mpc-scale distances.

We generated 21 evolutionary tracks of 200 time steps each, spanning a range of jet powers $Q = 10^{38.8}$–$10^{39.2}$ W. Propagating total length and radio luminosity uncertainties, we obtained $Q = 1.3 \pm 0.1 \times 10^{39}$ W and $T = 1.9^{+0.7}_{-0.2}$ Gyr. The jet power uncertainty of the outflow is set by radio luminosity uncertainty, whereas its age uncertainty is set by total length uncertainty. The inferred Gyr-scale age suggests that treating outflow evolution as a process at a single redshift—as is done at present in the model in ref. 28—is crude for the largest outflows and may need revision. The average speed of each jet $\langle\beta\rangle$ is $\frac{\langle v\rangle}{c} = \frac{l}{2cT} = 0.58^{+0.04}_{-0.07}\%$, in which c is the speed of light. The energy transported by the jets $E = QT = 7.6^{+2.1}_{-0.7}\times 10^{55}$ J. As a black hole can redirect at most half of the rest energy of infalling matter to electromagnetic radiation and jet fuelling, and the energy a RE AGN spends on electromagnetic radiation must at least equal the energy spent on jet fuelling, the black hole must have gained a mass $\Delta M_\bullet > 2\frac{E}{c^2} = 8.5^{+2.4}_{-0.8}\times 10^8\ M_\odot$ while powering the jets.

Total outflow length

To estimate the total length of Porphyrion from its projected length, we performed statistical deprojection. Equation 9 of ref. 14 stipulates the probability density function of an outflow's total length random variable L in case its projected length random variable L_p is known to equal some value l_p. This probability density function is parametrized by the tail index ξ of the Pareto distribution assumed to describe L. We calculate the median and expectation value of $L|L_p = l_p$ for tail indices $\xi = -3$ and $\xi = -4$, the integer values closest to the observationally favoured $\xi = -3.5 \pm 0.5$ (ref. 14).

First, we determined the cumulative distribution function (CDF) of $L|L_p = l_p$ through integration:

$$\begin{aligned} F_{L|L_p=l_p}(l) &= \int_{-\infty}^{l} f_{L|L_p=l_p}(l')\,\mathrm{d}l' \\ &= \frac{-\xi}{2^{1+\xi}\pi}\frac{\Gamma^2\left(-\frac{\xi}{2}\right)}{\Gamma(-\xi)}\int_1^{\max\{x,1\}} \frac{x'^{\xi-1}}{\sqrt{x'^2-1}}\mathrm{d}x', \end{aligned} \quad (2)$$

in which $x = \frac{l}{l_p}$ and $x' = \frac{l'}{l_p}$.

For $\xi = -3$, the CDF concretizes to

$$\begin{aligned} F_{L|L_p=l_p}(l) &= \frac{3}{2}\int_1^{\max\{x,1\}} \frac{\mathrm{d}x'}{x'^4\sqrt{x'^2-1}} \\ &= \begin{cases} 0 & \text{if } x < 1; \\ \dfrac{(2x^2+1)\sqrt{x^2-1}}{2x^3} & \text{if } x \geq 1. \end{cases} \end{aligned} \quad (3)$$

The median conditional total length, l_m, is defined by $F_{L|L_p=l_p}(l_m) = \frac{1}{2}$. Numerically, we obtain $x_m = \frac{l_m}{l_p} \approx 1.0664$, or $l_m \approx 1.0664 l_p$. As $l_p = 6.43 \pm 0.05$ Mpc, we find $l_m = 6.86 \pm 0.05$ Mpc. An analogous numerical determination of the 16th and 84th percentiles then yields $l = 6.9^{+1.6}_{-0.4}$ Mpc.

For $\xi = -4$, the CDF concretizes to

$$F_{L|L_p=l_p}(l) = \frac{16}{3\pi}\int_1^{\max\{x,1\}} \frac{dx'}{x'^5\sqrt{x'^2-1}} = \begin{cases} 0 & \text{if } x < 1; \\ \frac{2}{3\pi}\left(\frac{(3x^2+2)\sqrt{x^2-1}}{x^4} + 3\arccos\frac{1}{x}\right) & \text{if } x \geq 1. \end{cases} \quad (4)$$

Numerically, we obtain $x_m \approx 1.0515$, or $l_m \approx 1.0515 l_p$, and thus $l_m = 6.76 \pm 0.05$ Mpc. In the same way as before, we find $l = 6.8^{+1.2}_{-0.3}$ Mpc.

Equation 10 of ref. 14 gives a closed-form expression for $\mathbb{E}[L|L_p = l_p](\xi)$. Table 1 of the same work lists $\mathbb{E}[L|L_p = l_p](\xi = -3) = \frac{3\pi}{8} l_p$ and $\mathbb{E}[L|L_p = l_p](\xi = -4) = \frac{32}{9\pi} l_p$. In the case of Porphyrion, these expressions concretize to $\mathbb{E}[L|L_p = l_p](\xi = -3) = 7.58 \pm 0.06$ Mpc and $\mathbb{E}[L|L_p = l_p](\xi = -4) = 7.28 \pm 0.05$ Mpc.

By conditioning L on more knowledge than a value for L_p alone, statistical deprojection could be made more precise. For example, we could also condition on the fact that Porphyrion is generated by a Type 2 RE AGN. If Type 1 RE AGN are seen mostly face on and Type 2 RE AGN are seen mostly edge on, as proposed by the unification model (for example, ref. 17), then the detection of a Type 2 RE AGN would imply that the jets make a small angle with the sky plane. Extending the formulae to include this knowledge is beyond the scope of this work; however, mindful of the associated deprojection-factor-reducing effect, we choose $\xi = -4$ as our fiducial tail index.

To assess the transport capabilities of Porphyrion in a cosmological context, it is instructive to calculate its length relative to cosmic web length scales. In particular, the total length of the outflow relative to the typical cosmic void radius at its epoch is $f_v = l(1+z)R_v^{-1}$, in which R_v is the typical comoving cosmic void radius. For $l = 6.8^{+1.2}_{-0.3}$ Mpc, $z = 0.896 \pm 0.001$ and $R_v = 20$ Mpc (ref. 10), we find $f_v = 64^{+12}_{-3}\%$. For our fiducial total length $l = 7$ Mpc, we find $f_v = 66\%$.

Filament shape modification

We predict that powerful, long-lived outflows such as Porphyrion cause the filaments of their host galaxies to expand thermally. Through lateral shocks, the jets distribute an amount of heat Q_{WHIM} over the warm–hot IGM. This medium is sufficiently dilute such that plasma interactions can be neglected; as a result, the ideal gas law, $pV = Nk_BT$, may be adopted as the equation of state. Here, p, V, N and T are the filament's pressure, volume, plasma particle number and temperature, respectively, and k_B is Boltzmann's constant. Assuming a thermodynamic process at constant pressure and particle number, the work W is

$$W = p\Delta V = Nk_B\Delta T. \quad (5)$$

Before the emergence of the outflow, the equation of state of the filament is $pV_i = Nk_BT_i$, in which V_i and T_i are its initial volume and temperature, respectively. On dividing equation (5) by this equation of state, we obtain

$$\frac{\Delta V}{V_i} = \frac{\Delta T}{T_i}. \quad (6)$$

Assuming that the filament retains a cylindrical shape, initially with radius r_i and finally with radius r_f, and using that $\Delta V = V_f - V_i$, we obtain

$$\frac{r_f}{r_i} = \sqrt{1 + \frac{\Delta T}{T_i}}. \quad (7)$$

The radius ratio, $\frac{r_f}{r_i}$, depends only on the ratio between the temperature increase $\Delta T = T_f - T_i$ and the initial temperature. The temperature increase is

$$\Delta T = \frac{Q_{WHIM}}{NC_{p,m}}, \quad (8)$$

in which $C_{p,m}$ is the molar heat capacity at constant pressure. For a monatomic gas or a hydrogen plasma, $C_{p,m} = \frac{5}{2}R$, in which R is the molar gas constant. The number of filamentary electrons and atomic nuclei affected by the outflow is

$$N = \frac{\pi r_i^2 L \rho_i}{\mu m_p}, \quad (9)$$

in which L is the length of the cylindrical segment affected, ρ_i is the initial baryonic mass density, μ is the average mass of a plasma particle relative to the proton mass and m_p is the proton mass. We estimate $\frac{L}{2}$ by multiplying the typical speed of lateral shocks with the lifetime of the outflow. We decompose $\rho_i = \rho_{c,0}\Omega_{BM,0}(1+z)^3(1+\delta)$, in which z and δ are the cosmological redshift and baryonic overdensity of the filament, respectively.

To estimate Q_{WHIM} given E, the total energy carried by the jets up to the time of observation, we turn to analytical models and numerical simulations. Modelling indicates that roughly 10% of the total energy is lost through radiative processes[28]. This fraction increases with redshift, as inverse Compton losses to the cosmic microwave background become more pronounced. Numerical simulations show that, at least in galaxy clusters, about 50% of the non-radiated energy is converted into thermal or kinetic energy carried by the shocked medium and the other approximately 50% is converted into thermal or kinetic energy carried by the lobes of the outflow[64]. Over time, the kinetic energy turns into thermal energy. It is, at present, unclear how fast remnant lobes mix with the surrounding medium and how the mixing timescale varies with the density of the latter. Here we assume that, at late times, all of the energy of the lobes mixes with the surrounding medium. As such, we estimate $Q_{WHIM} \to 90\% \times E$.

We assess the outflow-induced morphological change to the filament by evaluating equation (7), taking $Q_{WHIM} = 7 \times 10^{55}$ J, $r_i \approx r_c = 1.2$ Mpc (a typical filament core radius[63]), $L = 2 \times 7$ Mpc $= 14$ Mpc (assuming that the region beyond the outflow's direct reach that is affected at late times is comparable in length with the outflow itself), $z = 0.9$, $1 + \delta = 10$, $\mu = 0.5$ and $T_i = 10^7$ K; we find $\Delta T = 3 \times 10^7$ K (an increase of about 300%) and $r_f = 2.4$ Mpc (an increase of about 100%). The heat dissipation of Porphyrion renders its native filament much hotter and thicker than it would have otherwise been.

For our cosmological outlook, we assumed a typical jet power and age that are each an order of magnitude lower than that of Porphyrion. We thus estimated the combined energy carried by 10 Mpc-scale outflows to be $Q_{WHIM} = 7 \times 10^{54}$ J. Assuming non-overlapping affected regions, we estimated $L = 10 \times 2 \times 1$ Mpc $= 20$ Mpc. Leaving all other parameters identical, we find $\Delta T = 2 \times 10^6$ K (an increase of about 20%) and $r_f = 1.3$ Mpc (an increase of about 10%).

Quasar-mass-based host galaxy candidate elimination

SDSS J152933.03+601552.5 is the quasar-hosting galaxy 19″ NNE of J152932.16+601534.4, the galaxy we have identified as the host of Porphyrion. We initially also considered SDSS J152933.03+601552.5 as a host galaxy candidate. However, aforementioned arguments involving the presence of jets and their orientation and, to a lesser degree, arguments involving core radio luminosity and core SSA all favour J152932.16+601534.4. We now discuss how our results would change if, instead, SDSS J152933.03+601552.5 were the host galaxy of Porphyrion. Doing so will lead to a contradiction that disproves this alternative hypothesis.

First, we discuss results that do not require dynamical modelling. To start, Porphyrion would remain generated by a RE AGN. The host galaxy redshift would decrease from $z = 0.896 \pm 0.001$ to $z = 0.799 \pm 0.001$, decreasing the projected length of Porphyrion from

$l_p = 6.43 \pm 0.05$ Mpc to $l_p = 6.21 \pm 0.05$ Mpc. Again using $\xi = -4$, the total length would decrease from $l = 6.8^{+1.2}_{-0.3}$ Mpc to $l = 6.5^{+1.2}_{-0.3}$ Mpc and its conditional expectation from $\mathbb{E}[L|L_p = l_p] = 7.28 \pm 0.05$ Mpc to $\mathbb{E}[L|L_p = l_p] = 7.03 \pm 0.06$ Mpc. If orientation distinguishes Type 1 from Type 2 RE AGN, as the unification model supposes, then these statistical deprojection results may underestimate the total length of Porphyrion. Porphyrion would remain the projectively longest galaxy-made structure identified so far. The stellar mass of the host would decrease from $M_\star = 6.7 \pm 1.4 \times 10^{11}\, M_\odot$ to $M_\star = 4.0^{+0.3}_{-0.3} \times 10^{11}\, M_\odot$, whereas the SFR would become $S = 4.9^{+0.3}_{-0.4} \times 10^1\, M_\odot\, \mathrm{yr}^{-1}$ (ref. 65). The total radio luminosity of Porphyrion at rest-frame wavelength $\lambda_r = 2$ m would decrease from $L_\nu = 2.8 \pm 0.3 \times 10^{26}$ W Hz^{-1} to $L_\nu = 2.2 \pm 0.2 \times 10^{26}$ W Hz^{-1}.

Next, we discuss results that come from dynamical modelling. The jet power would decrease from $Q = 1.3 \pm 0.1 \times 10^{39}$ W to $Q = 1.0 \pm 0.1 \times 10^{39}$ W, whereas the age would slightly increase from $T = 1.9^{+0.7}_{-0.2}$ Gyr to $T = 1.9^{+0.7}_{-0.1}$ Gyr. The transported energy would decrease from $E = 7.6^{+2.1}_{-0.7} \times 10^{55}$ J to $E = 6.4^{+1.8}_{-0.6} \times 10^{55}$ J and the minimum black hole mass gain from $\Delta M_\bullet > 8.5^{+2.4}_{-0.8} \times 10^8\, M_\odot$ to $\Delta M_\bullet > 7.2^{+2.0}_{-0.7} \times 10^8\, M_\odot$.

Finally, we arrive at a contradiction, as the SMBH mass of the quasar (measured from its SDSS BOSS spectrum) $M_\bullet = 2.5 \pm 0.3 \times 10^8\, M_\odot$ (ref. 66). This mass is lower than the minimum mass gain associated to the fuelling of Porphyrion's jets. Thus, assuming that SDSS J152933.03+601552.5 is the host galaxy of the outflow leads to a contradiction. This argument reaffirms that J152932.16+601534.4 is the host of Porphyrion.

Inclusion and ethics

We recognize that the Keck I telescope observations on which this work relies have been conducted from Maunakea, a site of high cultural and environmental significance for the Hawaiian people. We are grateful for the opportunity to collect data here and we support deepening astronomy's commitment to good stewardship of the mountain.

Data availability

The LoTSS DR2 is publicly available[68]. The authors share this work's proprietary LOFAR, uGMRT and Keck I telescope data, as well as the dynamical model runs and LoTSS–VLASS spectral indices, through Code Ocean.

Code availability

The dynamical model used to interpret the outflow is described by Hardcastle[28] and available for download[69]. Analysis and plotting code specific to this work is available on Code Ocean[70]. There are no access restrictions.

29. Planck Collaboration et al. Planck 2018 results. VI. Cosmological parameters. *Astron. Astrophys.* **641**, A6 (2020).
30. van Haarlem, M. P. et al. LOFAR: the LOw-Frequency ARray. *Astron. Astrophys.* **556**, A2 (2013).
31. Shimwell, T. W. et al. The LOFAR Two-metre Sky Survey. V. Second data release. *Astron. Astrophys.* **659**, A1 (2022).
32. Shimwell, T. W. et al. The LOFAR Two-metre Sky Survey. I. Survey description and preliminary data release. *Astron. Astrophys.* **598**, A104 (2017).
33. Tasse, C. et al. DDFacet: facet-based radio imaging package. Astrophysics Source Code Library, record ascl:2305.008 (2023).
34. van Weeren, R. J. et al. LOFAR observations of galaxy clusters in HETDEX. Extraction and self-calibration of individual LOFAR targets. *Astron. Astrophys.* **651**, A115 (2021).
35. Offringa, A. R. et al. WSCLEAN: an implementation of a fast, generic wide-field imager for radio astronomy. *Mon. Not. R. Astron. Soc.* **444**, 606–619 (2014).
36. Morabito, L. K. et al. Sub-arcsecond imaging with the International LOFAR Telescope. I. Foundational calibration strategy and pipeline. *Astron. Astrophys.* **658**, A1 (2022).
37. Jackson, N. et al. LBCS: the LOFAR Long-Baseline Calibrator Survey. *Astron. Astrophys.* **595**, A86 (2016).
38. Jackson, N. et al. Sub-arcsecond imaging with the International LOFAR Telescope. II. Completion of the LOFAR Long-Baseline Calibrator Survey. *Astron. Astrophys.* **658**, A2 (2022).
39. Gupta, Y. et al. The upgraded GMRT: opening new windows on the radio Universe. *Curr. Sci.* **113**, 707–714 (2017).
40. Intema, H. T. SPAM: Source Peeling and Atmospheric Modeling. Astrophysics Source Code Library, record ascl:1408.006 (2014).
41. Mohan, N. & Rafferty, D. PyBDSF: Python Blob Detection and Source Finder. Astrophysics Source Code Library, record ascl:1502.007 (2015).
42. Blandford, R. D. & Znajek, R. L. Electromagnetic extraction of energy from Kerr black holes. *Mon. Not. R. Astron. Soc.* **179**, 433–456 (1977).
43. Alam, S. et al. The eleventh and twelfth data releases of the Sloan Digital Sky Survey: final data from SDSS-III. *Astrophys. J. Suppl. Ser.* **219**, 12 (2015).
44. Dey, A. et al. Overview of the DESI Legacy Imaging Surveys. *Astron. J.* **157**, 168 (2019).
45. Duncan, K. J. All-purpose, all-sky photometric redshifts for the Legacy Imaging Surveys Data Release 8. *Mon. Not. R. Astron. Soc.* **512**, 3662–3683 (2022).
46. Oke, J. B. et al. The Keck low-resolution imaging spectrometer. *Publ. Astron. Soc. Pac.* **107**, 375 (1995).
47. McCarthy, J. K. et al. in *Proc. SPIE Conference on Optical Astronomical Instrumentation* (ed. D'Odorico, S.) 81–92 (SPIE, 1998).
48. Steidel, C. C. et al. A survey of star-forming galaxies in the $1.4 \lesssim z \lesssim 2.5$ redshift desert: overview. *Astrophys. J.* **604**, 534–550 (2004).
49. Rockosi, C. et al. in *Proc. Ground-based and Airborne Instrumentation for Astronomy III* (eds McLean, I. S., Ramsay, S. K. & Takami, H.) 77350R (SPIE, 2010).
50. Prochaska, J. et al. PypeIt: the Python spectroscopic data reduction pipeline. *J. Open Source Softw.* **5**, 2308 (2020).
51. Dawson, K. S. et al. The Baryon Oscillation Spectroscopic Survey of SDSS-III. *Astron. J.* **145**, 10 (2013).
52. Chambers, K. C. et al. The Pan-STARRS1 surveys. Preprint at https://arxiv.org/abs/1612.05560 (2019).
53. Jarrett, T. H. et al. The Spitzer–WISE survey of the ecliptic poles. *Astrophys. J.* **735**, 112 (2011).
54. Calistro Rivera, G., Lusso, E., Hennawi, J. F. & Hogg, D. W. AGNfitter: a Bayesian MCMC approach to fitting spectral energy distributions of AGNs. *Astrophys. J.* **833**, 98 (2016).
55. Martínez-Ramírez, L. N. et al. AGNFITTER-RX: Modeling the radio-to-X-ray spectral energy distributions of AGNs. *Astron. Astrophys.* **688**, A46 (2024).
56. Pasini, T. et al. Radio galaxies in galaxy groups: kinematics, scaling relations, and AGN feedback. *Mon. Not. R. Astron. Soc.* **505**, 2628–2637 (2021).
57. Arnaud, M. et al. The universal galaxy cluster pressure profile from a representative sample of nearby systems (REXCESS) and the $Y_{SZ} - M_{500}$ relation. *Astron. Astrophys.* **517**, A92 (2010).
58. Sun, M. et al. The pressure profiles of hot gas in local galaxy groups. *Astrophys. J. Lett.* **727**, L49 (2011).
59. Cooke, R. J. & Fumagalli, M. Measurement of the primordial helium abundance from the intergalactic medium. *Nat. Astron.* **2**, 957–961 (2018).
60. Lovisari, L., Reiprich, T. H. & Schellenberger, G. Scaling properties of a complete X-ray selected galaxy group sample. *Astron. Astrophys.* **573**, A118 (2015).
61. Ricciardelli, E., Quilis, V. & Planelles, S. The structure of cosmic voids in a ΛCDM Universe. *Mon. Not. R. Astron. Soc.* **434**, 1192–1204 (2013).
62. Upton Sanderbeck, P. R., D'Aloisio, A. & McQuinn, M. J. Models of the thermal evolution of the intergalactic medium after reionization. *Mon. Not. R. Astron. Soc.* **460**, 1885–1897 (2016).
63. Tuominen, T. et al. An EAGLE view of the missing baryons. *Astron. Astrophys.* **646**, A156 (2021).
64. Hardcastle, M. J. & Krause, M. G. H. Numerical modelling of the lobes of radio galaxies in cluster environments. *Mon. Not. R. Astron. Soc.* **430**, 174–196 (2013).
65. Barrows, R. S., Comerford, J. M., Stern, D. & Assef, R. J. A catalog of host galaxies for WISE-selected AGN: connecting host properties with nuclear activity and identifying contaminants. *Astrophys. J.* **922**, 179 (2021).
66. Chen, Z.-F., Pan, D.-S., Pang, T.-T. & Huang, Y. A catalog of quasar properties from the Baryon Oscillation Spectroscopic Survey. *Astrophys. J. Suppl. Ser.* **234**, 16 (2018).
67. Sweijen, F. GitHub repository for legacystamps. https://github.com/tikk3r/legacystamps (2021).
68. LOFAR Collaboration. Website for LOFAR surveys data, including LoTSS DR2. https://lofar-surveys.org (2022).
69. Hardcastle, M. J. GitHub repository for 'A simulation-based analytic model of radio galaxies'. https://github.com/mhardcastle/analytic (2021).
70. Oei, M. S. S. L. Code Ocean capsule for 'Black hole jets on the scale of the cosmic web'. https://codeocean.com/capsule/3908804/tree (2024).
71. Lang, D., Hogg, D. W. & Schlegel, D. J. WISE photometry for 400 million SDSS sources. *Astron. J.* **151**, 36 (2016).
72. Gordon, Y. A. et al. A quick look at the 3 GHz radio sky. I. Source statistics from the Very Large Array Sky Survey. *Astrophys. J. Suppl. Ser.* **255**, 30 (2021).
73. Helfand, D. J., White, R. L. & Becker, R. H. The last of FIRST: the final catalog and source identifications. *Astrophys. J.* **801**, 26 (2015).

Acknowledgements M.S.S.L.O. and R.J.v.W. acknowledge support from the VIDI research programme with project number 639.042.729, which is financed by the Dutch Research Council (NWO). M.S.S.L.O. also acknowledges support from the CAS–NWO programme for radio astronomy with project number 629.001.024, which is financed by the NWO. In addition, M.S.S.L.O., R.T. and R.J.v.W. acknowledge support from the ERC Starting Grant ClusterWeb 804208. M.J.H. acknowledges support from the UK STFC (ST/V000624/1). R.T. is grateful for support from the UKRI Future Leaders Fellowship (grant MR/T042842/1). A.B. acknowledges financial support from the European Union - Next Generation EU. F.d.G. acknowledges support from the ERC Consolidator Grant ULU 101086378. The work of D.S. was carried out at the Jet Propulsion Laboratory, California Institute of Technology, under a contract with the National Aeronautics and Space Administration (NASA). We thank F. Sweijen for making available legacystamps[67]. We thank R. Caniato and J.H. Croston for illuminating discussions. LOFAR data products were provided by the LOFAR Surveys Key Science project (LSKSP[68]) and were derived from observations with the International LOFAR Telescope (ILT). LOFAR[30] is the LOw-Frequency ARray designed and constructed by ASTRON. It has observing, data-processing and data-storage facilities in several countries, which are owned by various parties (each with their own funding sources) and which are collectively operated by the ILT foundation under a joint

scientific policy. The efforts of the LSKSP have benefited from funding from the European Research Council, NOVA, NWO, CNRS-INSU, the SURF Co-operative, the UK Science and Technology Funding Council and the Jülich Supercomputing Centre. We thank the staff of the GMRT, who made these observations possible. The GMRT is run by the National Centre for Radio Astrophysics of the Tata Institute of Fundamental Research. Some of the data presented herein were obtained at the W. M. Keck Observatory, which is operated as a scientific partnership among the California Institute of Technology, the University of California and NASA. The Observatory was made possible by the generous financial support of the W. M. Keck Foundation.

Author contributions A.R.D.J.G.I.B.G. and M.S.S.L.O. discovered Porphyrion; M.J.H., assisted by citizen scientists, independently found the outflow as part of LOFAR Galaxy Zoo. M.S.S.L.O. coordinated the ensuing project. R.J.v.W., H.J.A.R. and M.J.H. advised M.S.S.L.O. throughout. A.B. re-reduced and imaged the 6.2″ and 19.8″ LOFAR data; R.J.v.W. contributed. R.T. reduced and imaged the 0.4″ LOFAR data. F.d.G. explored the use of LOFAR LBA data, which he reduced and imaged. M.S.S.L.O. wrote the uGMRT follow-up proposal. M.S.S.L.O. and H.T.I. reduced and imaged the uGMRT data. S.G.D., D.S. and H.J.A.R. were instrumental in securing Keck time (PI: S.G.D.). A.C.R. observed the host galaxy with the LRIS; A.C.R. and D.S. reduced the data. G.C.R. determined the SED and stellar mass of the host galaxy; M.S.S.L.O. contributed. M.J.H. determined core spectral indices of Mpc-scale outflows. M.S.S.L.O. determined the spurious association probability, the galaxy cluster distances and the circumgalactic cosmic web percentile. M.J.H. performed dynamical modelling; M.S.S.L.O. contributed. M.S.S.L.O. derived the deprojection and filament-heating formulae. M.S.S.L.O. wrote the article, with contributions from A.R.D.J.G.I.B.G., R.T. and A.C.R. All authors provided comments to improve the text.

Competing interests The authors declare no competing interests.

Additional information

Supplementary information The online version contains supplementary material available at https://doi.org/10.1038/s41586-024-07879-y.

Correspondence and requests for materials should be addressed to Martijn S. S. L. Oei.

Peer review information *Nature* thanks Francesco Massaro and the other, anonymous, reviewer(s) for their contribution to the peer review of this work. Peer reviewer reports are available.

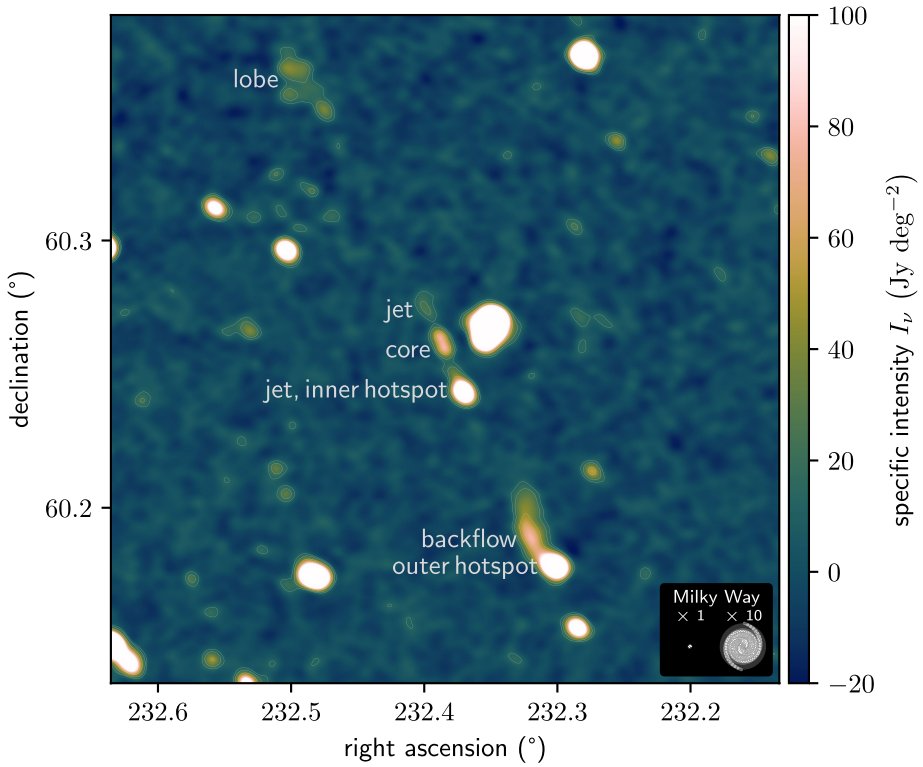

Extended Data Fig. 1 | ILT image of Porphyrion at a lower resolution of 19.8″. The image, again at central wavelength λ = 2.08 m, highlights diffuse emission in the northern lobe and southern backflow. We show the same sky region and annotations as in Fig. 1. The contours denote significance at fixed multiples of the image noise s.d. (σ): 3σ, 5σ and 10σ.

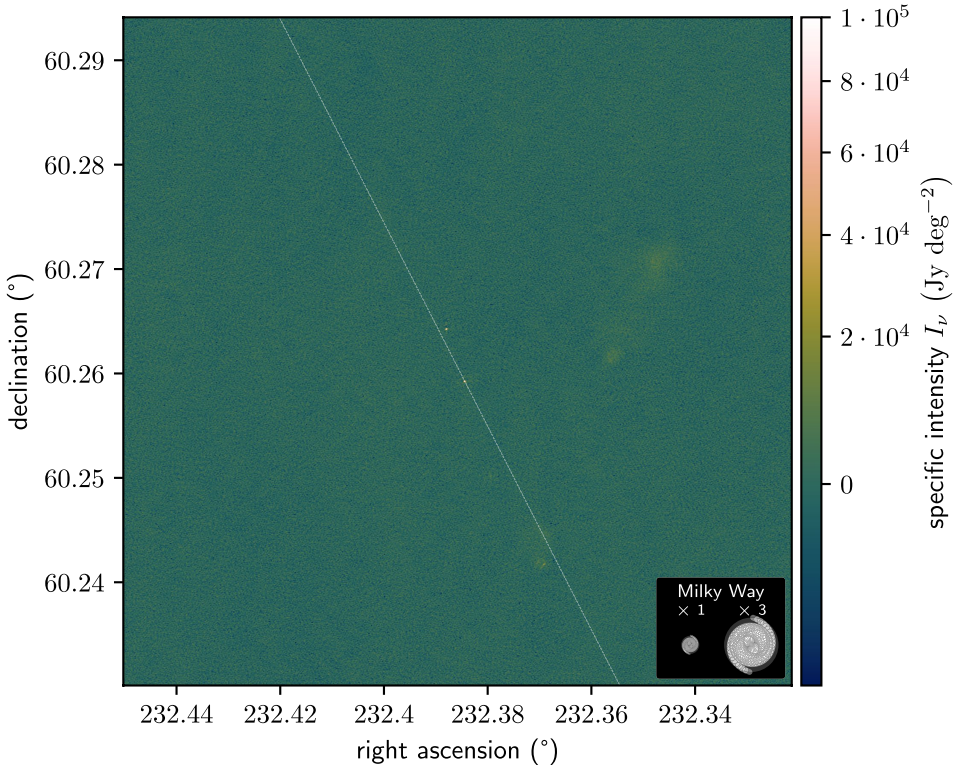

Extended Data Fig. 2 | VLBI close-up of the centre of Porphyrion. Our ILT image of Porphyrion's central 3.84′ × 3.84′ at $\lambda = 2.08$ m and 0.4″ resolution covers a third of the total jet system and reveals two radio-luminous AGN, detected at a significance of about 40σ (s.d.). We overlay the overarching jet axis (translucent white), determined from the northern lobe and southern hotspot (not shown), to scale for a jet radius of 1 kpc. The jet axis seems to pass through J152932.16+601534.4.

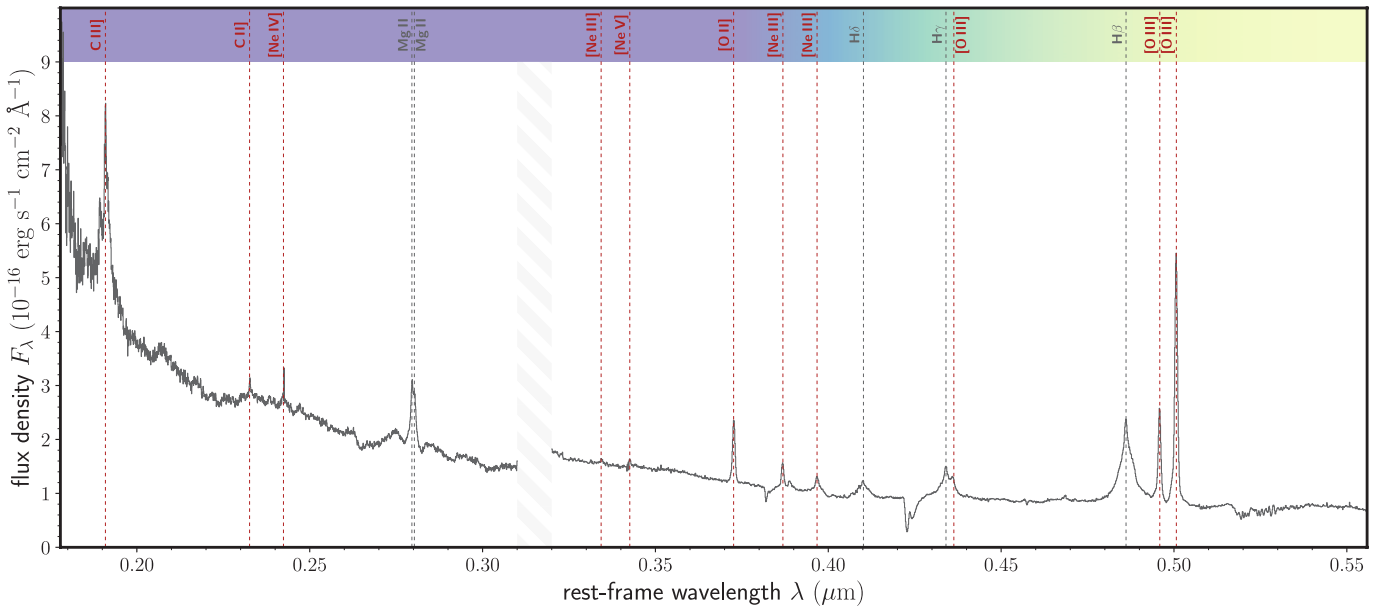

Extended Data Fig. 3 | Rest-frame ultraviolet–optical spectroscopy of J152933.03+601552.5. (This is the quasar-hosting galaxy 19″ NNE of the host galaxy of Porphyrion.) We identify redshifted hydrogen, carbon, oxygen, neon and magnesium lines, jointly implying $z_s = 0.799 \pm 0.001$. Forbidden lines from the narrow-line region of the quasar are shown in red. The spectrum has been measured with the LRIS on the W. M. Keck Observatory's Keck I telescope.

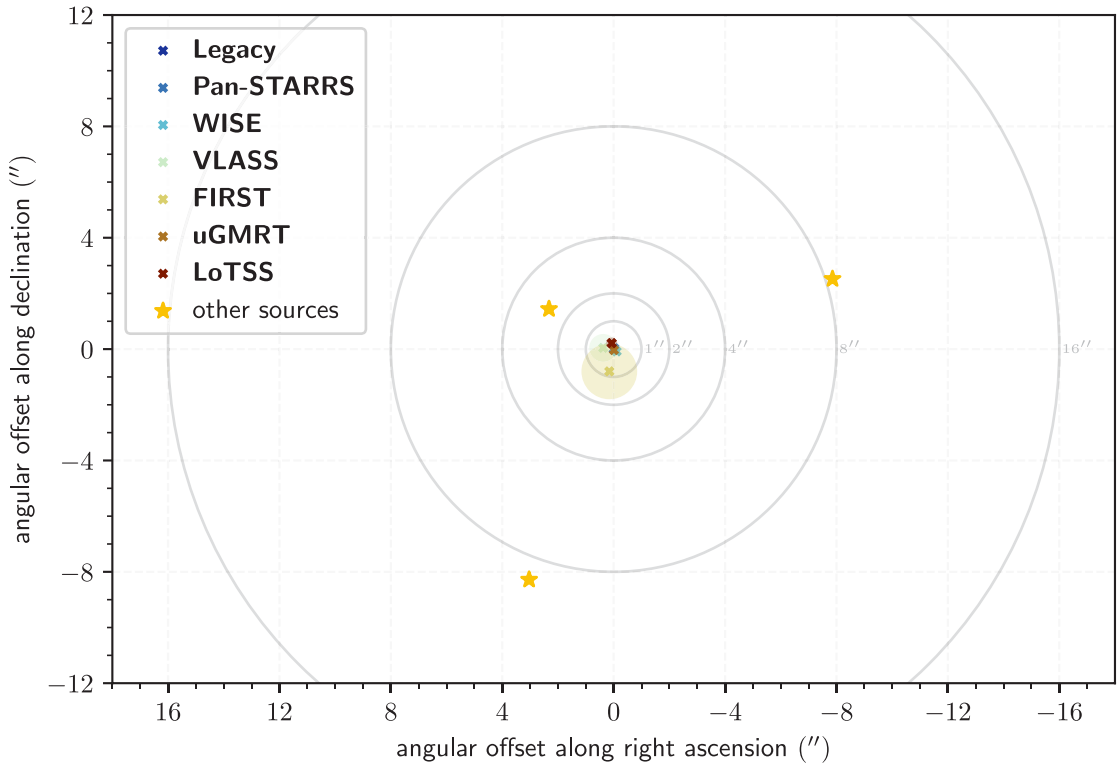

Extended Data Fig. 4 | Astrometric offsets for the host galaxy of Porphyrion. All flux densities used in the inference of the host galaxy SED occur within an arcsecond of the Legacy-Surveys-DR10-identified host position. Coloured disks show 1σ (s.d.) astrometric uncertainties and grey circles denote angular distances from the Legacy-Surveys-DR10-identified host position. The stars mark all other Legacy-Surveys-DR10-identified sources in the angular vicinity of Porphyrion's host.

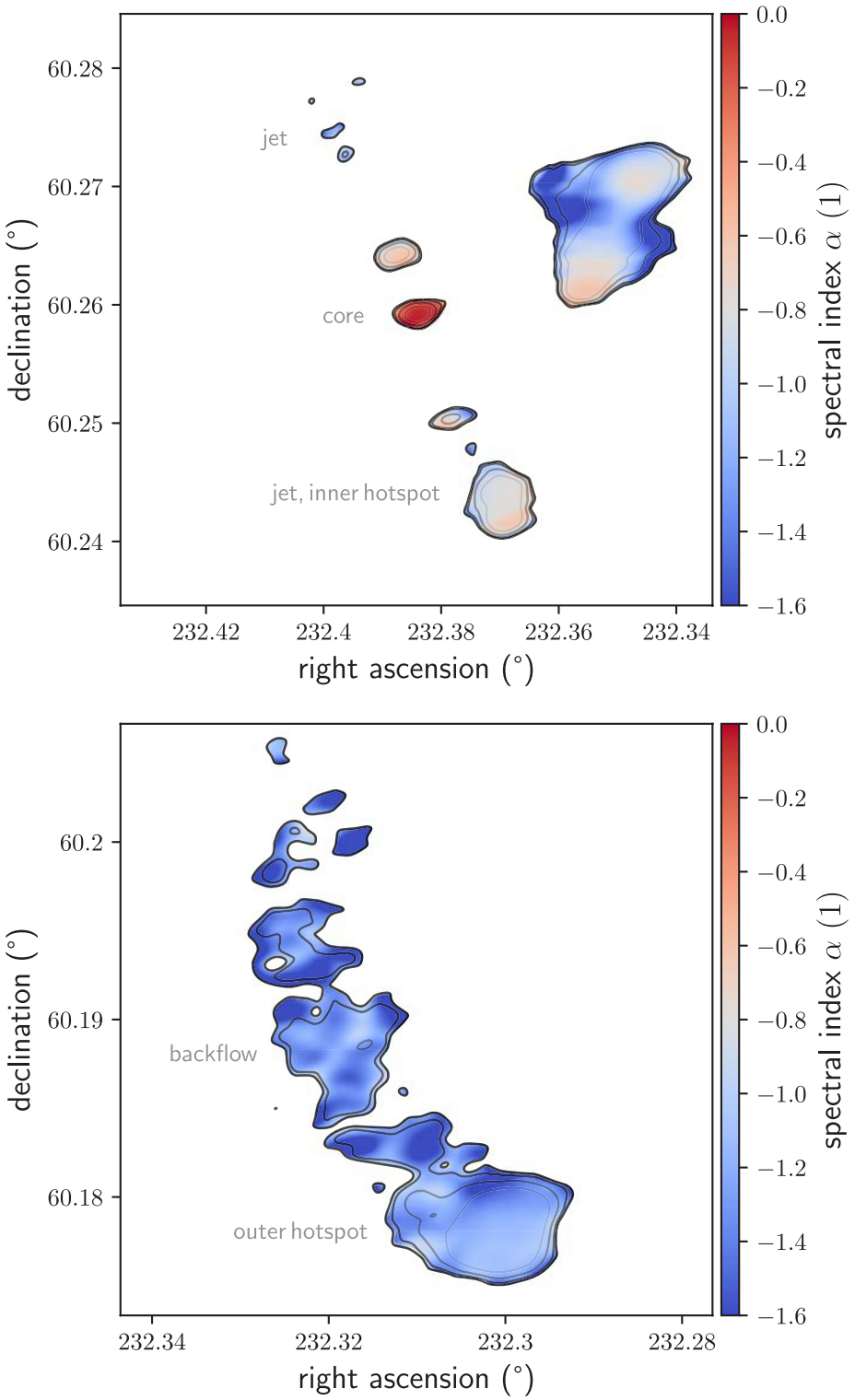

Extended Data Fig. 5 | Radio spectral indices around the centre and southern tip of Porphyrion. The top panel, which covers 3′ × 3′, reveals SSA at metre wavelengths in the host galaxy, consistent with the fuelling of powerful jets. The bottom panel, which covers 2′ × 2′, reveals a hotspot with backflow. We show effective spectral indices α between 0.46 and 2.08 m, at a resolution of 6.2″. From light to dark, the contours denote thermal-noise-induced spectral index uncertainties (s.d.) of 0.05, 0.1, 0.2 and 0.3.

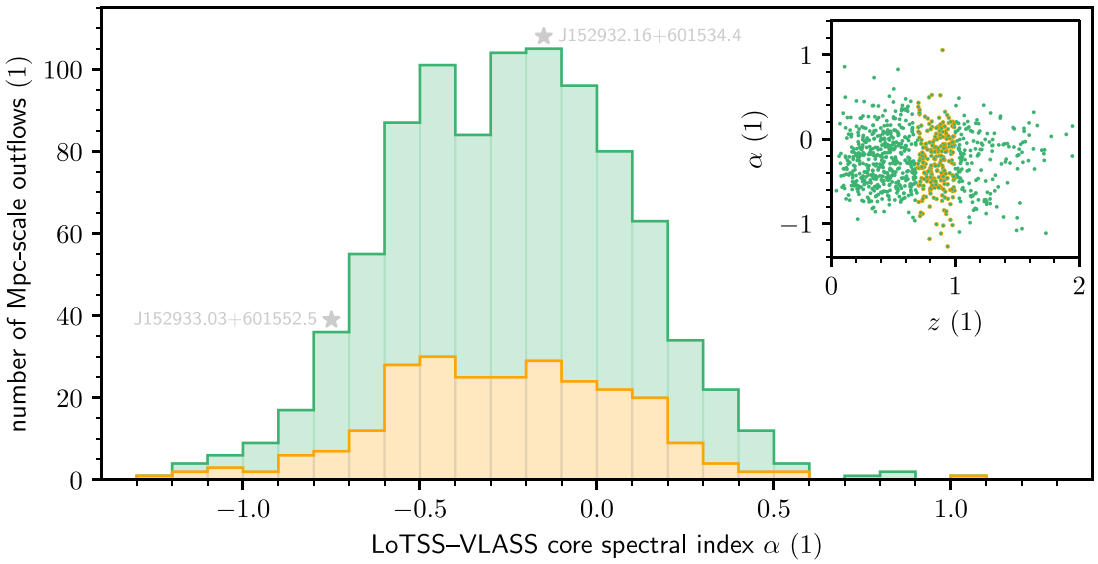

Extended Data Fig. 6 | Radio spectral index distributions of the cores of Mpc-scale outflows. Using LoTSS and VLASS data, we determined 924 effective spectral indices α between 0.1 and 2.08 m. In grey, we indicate the bins in which the core spectral indices of J152932.16+601534.4, the claimed host galaxy of Porphyrion, and J152933.03+601552.5 fall. The distribution suggests that the spectral index of J152932.16+601534.4 ($\alpha = -0.18 \pm 0.06$) is more typical of Mpc-scale outflows than the spectral index of J152933.03+601552.5. (For J152933.03+601552.5, owing to a VLASS non-detection, we show the LoTSS–uGMRT Band 4 spectral index.) The inset shows the same data as a function of redshift z. The orange subsample comprises Mpc-scale outflows whose redshifts differ at most $\Delta z = 0.1$ from those of either J152932.16+601534.4 or J152933.03+601552.5.

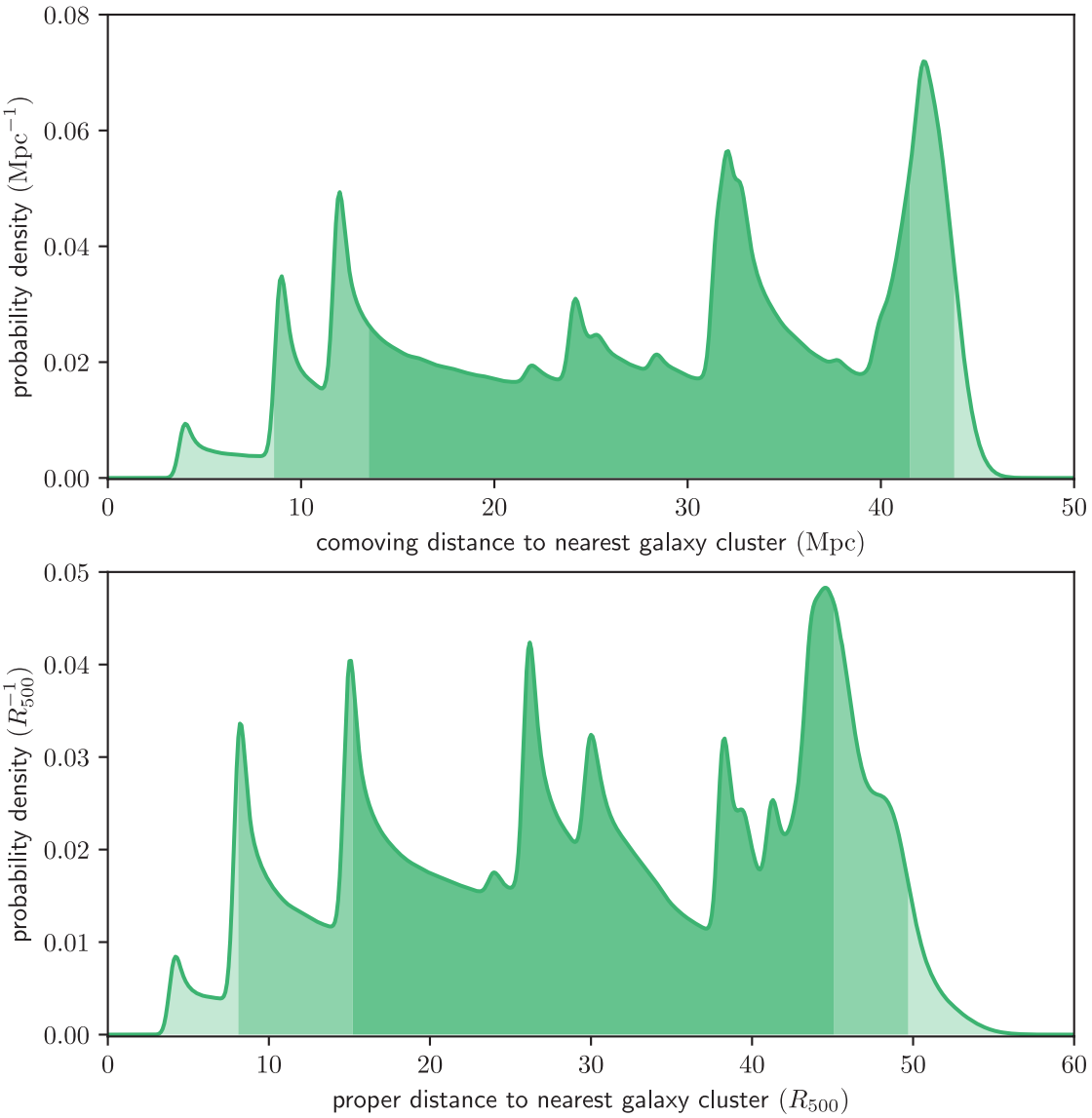

Extended Data Fig. 7 | Probabilistic analysis of the distance to the nearest cluster. DESI Legacy Imaging Surveys DR10 galaxy cluster redshift uncertainties induce multimodal, asymmetric probability distributions over measures of distance between the host galaxy of Porphyrion and the nearest galaxy cluster. We mark median-centred intervals containing 68% and 95% of all probability. The data suggest that Porphyrion does not originate from a cluster.

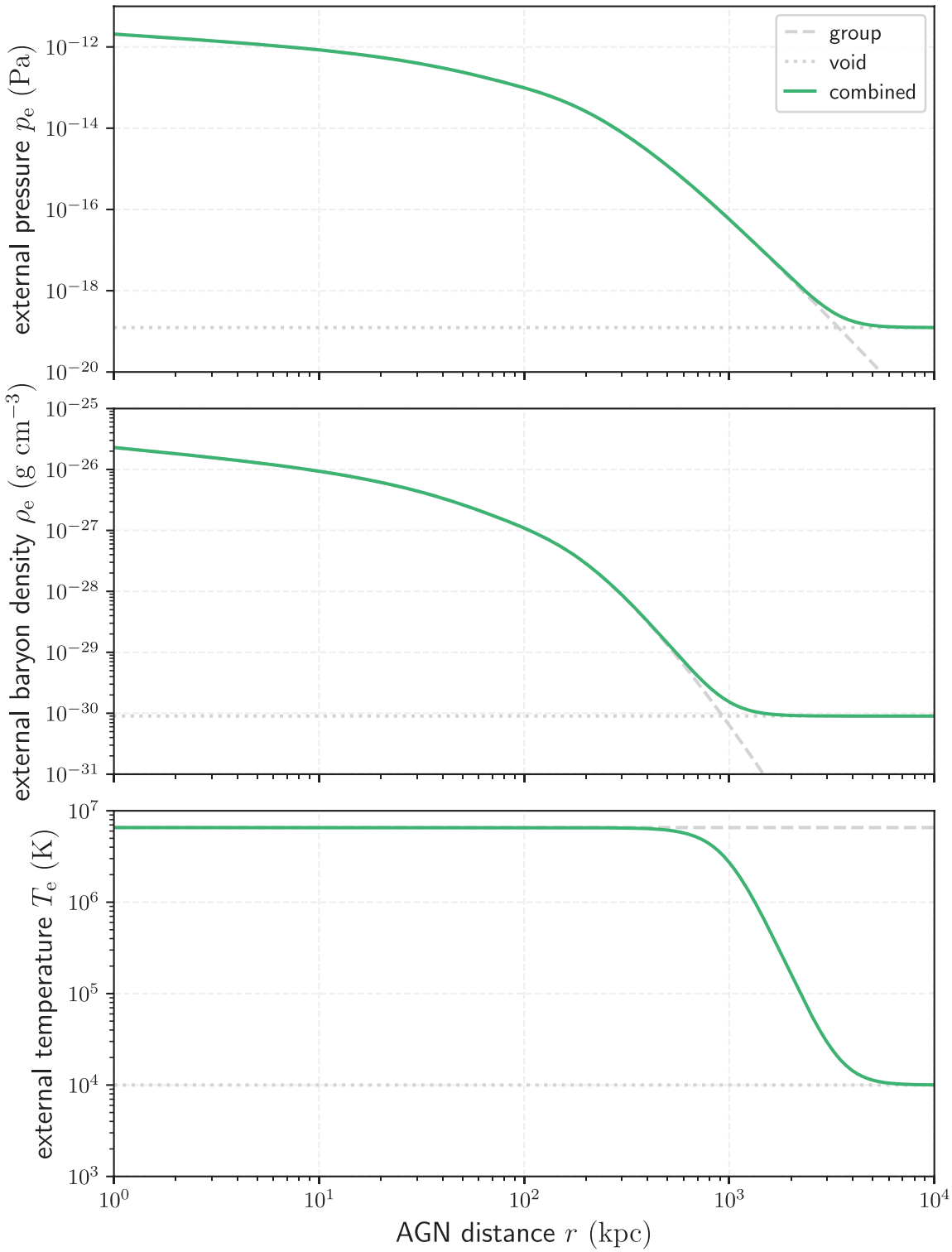

Extended Data Fig. 8 | Environmental profiles assumed in our dynamical modelling. We show the pressure, baryon density and temperature external to the outflow as a function of proper (rather than comoving) distance from the AGN of Porphyrion. The profiles consist of contributions from the presumed galaxy group of the outflow and the adjacent voids.

Extended Data Table 1 | Flux densities F_ν of Porphyrion's host galaxy

Band	λ (μm)	F_ν (Jy)	f_t (%)
Legacy *g*	$4.8 \cdot 10^{-1}$	$2.6 \pm 0.2 \cdot 10^{-6}$	96.3
Legacy *r*	$6.3 \cdot 10^{-1}$	$8.4 \pm 0.4 \cdot 10^{-6}$	97.5
Legacy *z*	$9.1 \cdot 10^{-1}$	$4.31 \pm 0.08 \cdot 10^{-5}$	98.6
Pan-STARRS *i*	$7.5 \cdot 10^{-1}$	$1.1 \pm 0.1 \cdot 10^{-5}$	98.0
Pan-STARRS *y*	$9.6 \cdot 10^{-1}$	$3.3 \pm 0.3 \cdot 10^{-5}$	98.7
WISE W1	$3.4 \cdot 10^{0}$	$2.41 \pm 0.02 \cdot 10^{-4}$	99.8
WISE W2	$4.6 \cdot 10^{0}$	$2.53 \pm 0.05 \cdot 10^{-4}$	99.9
WISE W3	$1.2 \cdot 10^{1}$	$8.1 \pm 0.5 \cdot 10^{-4}$	100
WISE W4	$2.2 \cdot 10^{1}$	$3.6 \pm 0.4 \cdot 10^{-3}$	100
VLASS	$1.0 \cdot 10^{5}$	$1.4 \pm 0.2 \cdot 10^{-3}$	100
FIRST	$2.1 \cdot 10^{5}$	$1.6 \pm 0.1 \cdot 10^{-3}$	100
uGMRT Band 4	$4.6 \cdot 10^{5}$	$2.1 \pm 0.1 \cdot 10^{-3}$	100
LoTSS	$2.1 \cdot 10^{6}$	$2.4 \pm 0.2 \cdot 10^{-3}$	100

These are as measured and thus have not been corrected for galactic extinction. To allow the reader to do so, we provide estimated galactic transmission fractions f_t. The uncertainties denote 1σ (s.d.). Entries are sorted by the central wavelengths λ of the observing bands, which cover the electromagnetic spectrum from the optical to the radio. When several flux densities or magnitudes from the same band were available in literature catalogues, we picked the highest signal-to-noise ratio measurement. Legacy data come from Dey et al.[44], Pan-STARRS data from Chambers et al.[52], WISE data from Lang et al.[71], VLASS data from Gordon et al.[72], FIRST data from Helfand et al.[73], uGMRT data from the present work and LoTSS data from Shimwell et al.[31].